



**HAL**  
open science

## The AMA1-RON complex drives Plasmodium sporozoite invasion in the mosquito and mammalian hosts

Priyanka Fernandes, Manon Loubens, Rémi Le Borgne, Carine Marinach, Beatrice Ardin, Sylvie Briquet, Laetitia Vincensini, Soumia Hamada, Bénédicte Hoareau-Coudert, Jean-Marc Verbavatz, et al.

### ► To cite this version:

Priyanka Fernandes, Manon Loubens, Rémi Le Borgne, Carine Marinach, Beatrice Ardin, et al.. The AMA1-RON complex drives Plasmodium sporozoite invasion in the mosquito and mammalian hosts. PLoS Pathogens, 2022, 18 (6), pp.e1010643. 10.1371/journal.ppat.1010643 . hal-03704136

**HAL Id: hal-03704136**

**<https://hal.sorbonne-universite.fr/hal-03704136v1>**

Submitted on 24 Jun 2022

**HAL** is a multi-disciplinary open access archive for the deposit and dissemination of scientific research documents, whether they are published or not. The documents may come from teaching and research institutions in France or abroad, or from public or private research centers.

L'archive ouverte pluridisciplinaire **HAL**, est destinée au dépôt et à la diffusion de documents scientifiques de niveau recherche, publiés ou non, émanant des établissements d'enseignement et de recherche français ou étrangers, des laboratoires publics ou privés.

1 **The AMA1-RON complex drives *Plasmodium* sporozoite invasion in the mosquito and**  
2 **mammalian hosts**

3

4 Priyanka Fernandes<sup>1</sup>✉, Manon Loubens<sup>1</sup>✉, Rémi Le Borgne<sup>2</sup>, Carine Marinach<sup>1</sup>, Beatrice  
5 Ardin<sup>1</sup>, Sylvie Briquet<sup>1</sup>, Laetitia Vincensini<sup>1</sup>, Soumia Hamada<sup>1,3</sup>, Bénédicte Hoareau-Coudert<sup>4</sup>,  
6 Jean-Marc Verbavatz<sup>2</sup>, Allon Weiner<sup>1</sup>, Olivier Silvie<sup>1\*</sup>

7

8 <sup>1</sup>Sorbonne Université, INSERM, CNRS, Centre d'Immunologie et des Maladies Infectieuses,  
9 CIMI-Paris, 75013, Paris, France

10 <sup>2</sup>Institut Jacques Monod, Université de Paris, CNRS, UMR 7592, 75205, Paris, France

11 <sup>3</sup>Sorbonne Université, INSERM, UMS PASS, Plateforme Post-génomique de la Pitié  
12 Salpêtrière (P3S), 75013, Paris, France

13 <sup>4</sup>Sorbonne Université, INSERM, UMS PASS, Plateforme de cytométrie de la Pitié-Salpêtrière  
14 (CyPS), 75013, Paris, France

15

16 ✉These authors contributed equally to the work.

17

18 \*Corresponding author: [olivier.silvie@inserm.fr](mailto:olivier.silvie@inserm.fr).

19

20

21

22

23

24 Running head: AMA1-RON complex in *Plasmodium* sporozoites

25

26 Keywords: *Plasmodium*; malaria; sporozoites; conditional mutagenesis; AMA1; RONS.

27

28

29 **Abstract**

30 *Plasmodium* sporozoites that are transmitted by blood-feeding female *Anopheles* mosquitoes  
31 invade hepatocytes for an initial round of intracellular replication, leading to the release of  
32 merozoites that invade and multiply within red blood cells. Sporozoites and merozoites share  
33 a number of proteins that are expressed by both stages, including the Apical Membrane  
34 Antigen 1 (AMA1) and the Rhoptry Neck Proteins (RONs). Although AMA1 and RONs are  
35 essential for merozoite invasion of erythrocytes during asexual blood stage replication of the  
36 parasite, their function in sporozoites was still unclear. Here we show that AMA1 interacts with  
37 RONs in mature sporozoites. By using DiCre-mediated conditional gene deletion in *P. berghei*,  
38 we demonstrate that loss of AMA1, RON2 or RON4 in sporozoites impairs colonization of the  
39 mosquito salivary glands and invasion of mammalian hepatocytes, without affecting  
40 transcellular parasite migration. Three-dimensional electron microscopy data showed that  
41 sporozoites enter salivary gland cells through a ring-like structure and by forming a transient  
42 vacuole. The absence of a functional AMA1-RON complex led to an altered morphology of the  
43 entry junction, associated with epithelial cell damage. Our data establish that AMA1 and RONs  
44 facilitate host cell invasion across *Plasmodium* invasive stages, and suggest that sporozoites  
45 use the AMA1-RON complex to efficiently and safely enter the mosquito salivary glands to  
46 ensure successful parasite transmission. These results open up the possibility of targeting the  
47 AMA1-RON complex for transmission-blocking antimalarial strategies.

48

49

50 **Author summary**

51 Malaria is caused by *Plasmodium* parasites, which are transmitted by mosquitoes. Infectious  
52 stages of the parasite known as sporozoites colonize the mosquito salivary glands and are  
53 injected into the host when the insect probes the skin for blood feeding. Sporozoites rapidly  
54 migrate to the host liver, invade hepatocytes and differentiate into the next invasive forms, the  
55 merozoites, which invade and replicate inside red blood cells. Merozoites invade cells through  
56 a specialized structure, known as the moving junction, formed by proteins called AMA1 and  
57 RONs. The role of these proteins in sporozoites remains unclear. Here we used conditional  
58 genome editing in a rodent malaria model to generate AMA1- and RON-deficient sporozoites.  
59 Phenotypic analysis of the mutants revealed that sporozoites use the AMA1-RON complex  
60 twice, first in the mosquito to safely enter the salivary glands and ensure successful parasite  
61 transmission, then in the mammalian host liver to establish a replicative niche. Our data  
62 establish that AMA1 and RONs facilitate host cell invasion across *Plasmodium* invasive  
63 stages, and might represent potential targets for transmission-blocking antimalarial strategies.

64

65

## 66 **Introduction**

67 Host cell invasion is an obligatory step in the *Plasmodium* life cycle. There are several  
68 invasive stages of *Plasmodium*, each equipped with its own set of specialized secretory  
69 organelles and proteins that facilitate invasion into or through host cells. Invasive stages of  
70 Apicomplexa typically invade target host cells actively by gliding through a structure known as  
71 the moving junction (MJ), which consists of a circumferential zone of close apposition of  
72 parasite and host cell membranes. Studies with *Toxoplasma gondii* tachyzoites and  
73 *Plasmodium falciparum* merozoites have shown that formation of the MJ involves the export  
74 of rhoptry neck proteins RONs into the host cell, where RON2 is inserted into the host cell  
75 membrane and serves as a receptor for the Apical Membrane Antigen 1 (AMA1), that is  
76 secreted from the micronemes onto the surface of the parasite [1–3]. Formation of the MJ is  
77 associated with active penetration inside the parasitophorous vacuole (PV), which is essential  
78 for further development and replication of the parasite.

79 Although the AMA1-RON2 interaction seems to be conserved across the phylum of  
80 Apicomplexa, its role in *Plasmodium* sporozoites is controversial. *Plasmodium* sporozoites  
81 express AMA1 and the RON proteins RON2, RON4 and RON5 [4–10]. Two studies reported  
82 that AMA1 is not essential for development in the mosquito and during hepatocyte invasion in  
83 *P. berghei*, while RON4 in contrast was shown to be essential for hepatocyte invasion,  
84 suggesting independent roles for AMA1 and RON proteins in sporozoites [7,11]. However,  
85 both polyclonal antibodies against AMA1 [4] and the R1 peptide inhibitor of AMA1 [12],  
86 effectively reduced hepatocyte invasion by *P. falciparum* sporozoites [13]. More recently, a  
87 promoter swap strategy was employed to knockdown RONs in *P. berghei* sporozoites,  
88 uncovering an unexpected role of these proteins during invasion of the mosquito salivary  
89 glands [14,15]. Owing to these conflicting data, the precise role of AMA1 and RONs in  
90 *Plasmodium* sporozoites is uncertain.

91 As conventional reverse genetics cannot be used to target AMA1 and RONs, due to their  
92 essential nature in asexual blood stages, previous studies relied on conditional approaches  
93 such as the Flippase (FLP)/Flp recombination target (FRT) system [7] or promoter swap

94 strategies [14] to target these genes. The rapamycin inducible DiCre recombinase system, first  
95 introduced to apicomplexan research in *T. gondii* [16] and *P. falciparum* [17], has recently  
96 emerged as a potent method of gene inactivation in different developmental stages of *P.*  
97 *falciparum* [18] and *P. berghei* [19]. We recently described a fluorescent DiCre-expressing  
98 parasite line in *P. berghei* and showed that efficient and complete gene excision can be  
99 induced in asexual blood stages and also sporozoites [19]. In this study, we used the DiCre  
100 system to achieve conditional deletion of *ama1*, *ron2* and *ron4* genes in *P. berghei* sporozoites.  
101 Our data reveal that sporozoites rely on AMA1 and RONs to invade salivary glands in the  
102 mosquito and hepatocytes in the mammalian host, implying a conserved feature of the invasion  
103 process across invasive stages of *Plasmodium*.

104

105

106 **Results**

107 **Deletion of *ama1* 3'UTR is not sufficient to abrogate AMA1 expression in *P. berghei***

108 To ablate AMA1 protein expression in *P. berghei*, we first decided to conditionally delete  
109 the 3' untranslated region (UTR) of *ama1* using the DiCre method, as previously reported with  
110 the FLP/FRT system [7]. We floxed the 3'UTR of *ama1*, together with a GFP and an hDHFR  
111 marker, to generate the *ama1* $\Delta$ utr parasite line in the mCherry-expressing PbDiCre parasite  
112 background [19] (**Figs 1A** and **S1A**). To exclude any unspecific effects arising from  
113 modification of the *ama1* locus, we also generated a control parasite line (*ama1*Con) where  
114 we introduced the LoxN sites downstream of the 3' UTR (**Figs 1B** and **S2A**). After transfection  
115 and selection with pyrimethamine, pure populations of recombinant parasites were sorted by  
116 flow cytometry and genotyped by PCR to confirm correct genomic integration of the constructs  
117 and to exclude the presence of any residual unmodified PbDiCre parasites (**S1B** and **S2B**  
118 **Figs**).

119

120

121 **Fig 1. Deletion of the 3' UTR of *ama1* has no phenotypical impact in *P. berghei***

122 **A-B.** Strategy to generate *ama1* $\Delta$ utr (A) and *ama1*Con (B) parasites by modification of the wild  
123 type *ama1* locus in PbDiCre parasites. **C-D.** Blood stage growth of untreated and rapamycin-  
124 treated *ama1* $\Delta$ utr (C) or *ama1*Con (D) parasites. Rapamycin was administered at day 2. The  
125 graphs represent the parasitaemia (mean +/- SEM) in groups of 3 mice. **E.**  
126 Immunofluorescence staining of rapamycin-treated *ama1*Con and *ama1* $\Delta$ utr blood stage  
127 schizonts with anti-AMA1 antibodies (blue). The right panels show mCherry (red), GFP (green)  
128 and AMA1 (blue) merged images. Scale bar = 10  $\mu$ m. **F.** Immunofluorescence images of  
129 rapamycin-treated *ama1*Con and *ama1* $\Delta$ utr sporozoites after staining with anti-AMA1  
130 antibodies (magenta). The right panels show Hoechst (blue) and AMA1 (magenta) merged  
131 images. Scale bar = 5  $\mu$ m.

132

133

134 We next analyzed the effects of rapamycin on *ama1*Con and *ama1* $\Delta$ utr parasites during  
135 blood stage growth (**Figs 1C** and **1D**), by quantifying the percentage of excised  
136 (mCherry<sup>+</sup>/GFP<sup>-</sup>) and non-excised (mCherry<sup>+</sup>/GFP<sup>+</sup>) parasites by flow cytometry (**S1C** and  
137 **S2C Figs**). In the *ama1*Con infected group, rapamycin treatment induced complete excision  
138 of the floxed GFP cassette (**S2C Fig**), which, as expected, had no significant effect on parasite  
139 growth and multiplication in the blood, which was comparable to the untreated group (**Fig 1D**).  
140 Excision of the GFP cassette was also confirmed by genotyping PCR (**S2B Fig**). Surprisingly,  
141 rapamycin treatment of the *ama1* $\Delta$ utr infected group also had no effect on both parasite growth  
142 and multiplication in the blood (**Fig 1C**), despite efficient DNA excision based on  
143 disappearance of the GFP cassette after rapamycin treatment (**S1C Fig**). Genotyping of  
144 mCherry<sup>+</sup>/GFP<sup>-</sup> parasites by PCR and sequencing of the locus after excision confirmed that  
145 the 3'UTR had been excised in rapamycin-treated *ama1* $\Delta$ utr parasites, excluding any  
146 contamination with parental PbDiCre (**S1B Fig**).

147 We next examined rapamycin-treated *ama1*Con and *ama1* $\Delta$ utr blood-stage schizonts by  
148 immunofluorescence staining with anti-AMA1 antibodies. Intriguingly, we observed AMA1  
149 expression in both *ama1*Con and *ama1* $\Delta$ utr merozoites after rapamycin exposure (**Fig 1E**),  
150 implying that deletion of the *ama1* 3'UTR alone was not sufficient to abrogate expression of  
151 the protein in merozoites. We further analyzed the impact of 3'UTR deletion on AMA1  
152 expression in sporozoites. For this purpose, *ama1*Con and *ama1* $\Delta$ utr parasites were treated  
153 with rapamycin or left untreated and then transmitted to mosquitoes, as described previously  
154 [19]. Deletion of the *ama1* 3'UTR in *ama1* $\Delta$ utr parasites had no impact on oocyst formation in  
155 the midgut or sporozoite invasion of salivary glands, which were comparable to untreated  
156 *ama1* $\Delta$ utr and both rapamycin-treated and untreated *ama1*Con parasites (**S3 Fig**). As  
157 observed in merozoites, AMA1 protein was also detected in salivary gland sporozoites from  
158 rapamycin-treated *ama1* $\Delta$ utr by immunofluorescence, similar to *ama1*Con parasites (**Fig 1F**).  
159 We conclude from these data that deletion of the 3'UTR of *ama1* is not sufficient to abrogate  
160 AMA1 protein expression and cause phenotypical changes in *P. berghei* merozoites and  
161 sporozoites.



162

### 163 **Complete conditional gene deletion of *ama1* in *P. berghei***

164 Since deletion of the 3'UTR was insufficient to deplete AMA1, we decided to delete the  
165 full-length *ama1* gene, by placing LoxN sites both upstream and downstream of the gene (**Fig**  
166 **2A**). One intrinsic feature of the Cre Lox system is the retention of a Lox site following  
167 recombination. We therefore reused rapamycin-treated *ama1*Con parasites, which contained  
168 a single LoxN site downstream of *ama1* 3'UTR and had excised the GFP-hDHFR marker (**Fig**  
169 **1B**), and transfected these parasites with the *ama1*cKO construct designed to introduce a  
170 second LoxN site upstream of the *ama1* gene, together with a GFP-hDHFR cassette (**Figs 2A**  
171 and **S4A**). Following transfection, the resulting *ama1*cKO parasites were sorted by FACS and  
172 genotyped to confirm correct integration of the construct into the genome and verify the  
173 absence of any residual unmodified *ama1*Con parasites (**S4B Fig**). We then evaluated the  
174 effect of rapamycin treatment on blood-stage growth of *ama1*cKO parasites, by injecting mice  
175 with 10<sup>6</sup> pRBCs and treating them with a single oral dose of rapamycin. In contrast to untreated  
176 parasites, *ama1*cKO parasite growth was abrogated in mice upon rapamycin exposure (**Fig**  
177 **2B**), thus confirming efficient gene deletion and the essential role of AMA1 in merozoite  
178 invasion and parasite survival in the blood. Genotyping by PCR confirmed *ama1* gene excision  
179 in rapamycin-exposed *ama1*cKO parasites, but also revealed the persistence of non-excised  
180 parasites 2 and 6 days after rapamycin treatment (**S4C Fig**), which eventually outcompeted  
181 the excised population.

182

183

### 184 **Fig 2. AMA1 is required during *P. berghei* invasion of mosquito salivary glands**

185 **A.** Strategy to generate *ama1*cKO parasites by modification of the *ama1* locus in rapamycin-  
186 treated *ama1*Con parasites. **B.** Blood stage growth of rapamycin-treated and untreated  
187 *ama1*cKO parasites. The graph represents the parasitaemia (mean +/- SEM) in groups of 3  
188 mice. Rapamycin was administered at day 2. \*\*, p < 0.01; \*\*\*\*, p < 0.0001 (Two-way ANOVA).  
189 **C-E.** Quantification of midgut sporozoites (MG-SPZ, C), salivary gland sporozoites (SG-SPZ,

190 D) or haemolymph sporozoites (HL-SPZ, E) isolated from mosquitoes infected with untreated  
191 or rapamycin-treated *ama1Con* and *ama1cKO* parasites. The graphs show the number of  
192 sporozoites per female mosquito (mean +/- SEM). Each dot represents the mean value  
193 obtained in independent experiments after dissection of 30-50 mosquitoes (MG, HL) or 50-70  
194 mosquitoes (SG), respectively. Ns, non-significant; \*\*\*\*,  $p < 0.0001$  (One-way ANOVA followed  
195 by Tukey's multiple comparisons test). **F-H.** Quantification of excised (mCherry<sup>+</sup>/GFP<sup>-</sup>, red)  
196 and non-excised (mCherry<sup>+</sup>/GFP<sup>+</sup>, green) midgut sporozoites (MG-SPZ, F), salivary gland  
197 sporozoites (SG-SPZ, G) or haemolymph sporozoites (HL-SPZ, H) isolated from mosquitoes  
198 infected with untreated or rapamycin-treated *ama1Con* and *ama1cKO* parasites. **I.**  
199 Immunofluorescence imaging of untreated and rapamycin-treated *ama1cKO* salivary gland  
200 sporozoites after staining with anti-AMA1 antibodies (magenta). The right panels show  
201 Hoechst (blue) and AMA1 (magenta) merged images. Scale bar = 5  $\mu$ m. **J.** Quantification of  
202 AMA1-positive and AMA1-negative sporozoites among untreated or rapamycin-exposed  
203 *ama1Con*, *ama1 $\Delta$ utr* and *ama1cKO* sporozoites, as assessed by microscopy.

204

205

## 206 **AMA1 is required for sporozoite invasion of the mosquito salivary glands**

207 In order to determine the function of AMA1 in sporozoites, we transmitted rapamycin-  
208 treated and untreated *ama1cKO* parasites to mosquitoes, 24 hours after rapamycin treatment.  
209 In parallel, mosquitoes were fed with rapamycin-treated and untreated *ama1Con* parasites as  
210 a reference line. Both rapamycin-treated and untreated *ama1cKO* parasites were capable of  
211 colonising the mosquito midgut (**S5 Fig**), comparable to *ama1Con* parasites (**S3 Fig**). Despite  
212 no difference in the levels of exflagellation between the parasite lines and treatment conditions,  
213 we observed a slight reduction in the number of midgut sporozoites for rapamycin-exposed  
214 *ama1cKO* parasites, which however was not statistically significant (**Fig 2C**). Importantly,  
215 quantification of the percentage of excised (mCherry<sup>+</sup>/GFP<sup>-</sup>) and non-excised  
216 (mCherry<sup>+</sup>/GFP<sup>+</sup>) parasites revealed close to 100% gene excision in sporozoites isolated from

217 the midguts of mosquitoes infected with rapamycin-treated *ama1Con* and *ama1cKO* parasites  
218 **(Fig 2F)**.

219 In the next step, we quantified sporozoites isolated from the salivary glands of infected  
220 mosquitoes and observed no difference between mosquitoes infected with untreated  
221 *ama1Con* or *ama1cKO* parasites **(Fig 2D)**. In sharp contrast, the number of salivary gland  
222 sporozoites isolated from rapamycin-treated *ama1cKO* infected mosquitoes was severely  
223 reduced as compared to untreated parasites **(Fig 2D)**. As expected, we could only observe  
224 mCherry<sup>+</sup>/GFP<sup>+</sup> (non-excised) salivary gland sporozoites in untreated *ama1Con* and  
225 *ama1cKO* parasites, while rapamycin-treated *ama1Con* and *ama1cKO* sporozoites were  
226 mCherry<sup>+</sup>/GFP<sup>-</sup> (excised) **(Figs 2G and S5B)**. Interestingly, a small proportion (<10%) of  
227 *ama1cKO*<sup>rapa</sup> salivary gland sporozoites were mCherry<sup>+</sup>/GFP<sup>+</sup> (non-excised), suggesting an  
228 enrichment of sporozoites harbouring an intact *ama1* gene, in the salivary glands of infected  
229 mosquitoes **(Fig 2G)**.

230 In order to determine if a defect in egress from oocysts or invasion of the salivary glands  
231 was the reason behind the reduction in *ama1cKO*<sup>rapa</sup> salivary gland sporozoite numbers, we  
232 quantified haemolymph sporozoites from infected mosquitoes at day 14 post infection. There  
233 was no significant difference between the numbers of haemolymph sporozoites isolated from  
234 *ama1Con* and *ama1cKO* infected mosquitoes with or without rapamycin treatment **(Fig 2E)**.  
235 Using microscopy, we could only see non-excised (mCherry<sup>+</sup>/GFP<sup>+</sup>) haemolymph sporozoites  
236 for untreated *ama1Con*- and *ama1cKO*-infected mosquitoes, while all rapamycin-treated  
237 *ama1Con* and *ama1cKO* haemolymph sporozoites were excised (mCherry<sup>+</sup>/GFP<sup>-</sup>) **(Fig 2H)**.  
238 The absence of a defect in egress from oocysts was also documented by microscopy imaging  
239 of the abdomen of infected mosquitoes, where scavenging of circulating sporozoites following  
240 egress results in bright red fluorescence of pericardial cellular structures **(S6 Fig)**. A similar  
241 percentage of mosquitoes displayed mCherry-labelled pericardial cells between untreated and  
242 rapamycin treated *ama1Con* and *ama1cKO* infected mosquitoes, confirming that loss of AMA1  
243 expression in sporozoites does not affect sporozoite egress from oocysts **(S6 Fig)**.

244 Lastly, we verified the loss of AMA1 expression in sporozoites by immunofluorescence  
245 imaging of salivary gland sporozoites using anti-AMA1 antibodies. AMA1 was detected in  
246 untreated *ama1cKO* sporozoites and untreated and rapamycin-treated *ama1Con* sporozoites,  
247 with a typical micronemal distribution (**Figs 1F and 2I**). However, no AMA1 was detected in  
248 *ama1cKO* sporozoites after rapamycin treatment, indicating the loss of AMA1 (**Fig 2I**).  
249 Quantification of AMA1 expression showed that all sporozoites from *ama1Con* and *ama1 $\Delta$ utr*  
250 expressed AMA1, irrespective of rapamycin exposure, similar to untreated *ama1cKO*  
251 sporozoites (**Fig 2J**). In contrast, >95% of the sporozoites isolated from mosquitoes infected  
252 with rapamycin-treated *ama1cKO* parasites lacked AMA1 expression, confirming successful  
253 gene deletion and protein depletion (**Fig 2J**). Overall, our results demonstrate that loss of  
254 AMA1 expression in sporozoites impairs invasion of the mosquito salivary glands, without  
255 affecting development or egress from oocysts.

256

### 257 **AMA1 is required for efficient sporozoite invasion of hepatocytes**

258 In the next step, we tested if AMA1-deficient salivary gland sporozoites could infect  
259 hepatocytes. AMA1 was previously suggested to be implicated in cell traversal of *P. falciparum*  
260 sporozoites [13]. Hence we first verified if *ama1* gene excision in *P. berghei* affected sporozoite  
261 cell traversal *in vitro*, using a dextran assay as previously described [20]. Quantification of  
262 dextran-positive cells indicated that cell traversal was comparable between *ama1Con* and  
263 *ama1cKO* rapamycin-treated parasites, implying that both motility and cell traversal activity of  
264 salivary gland sporozoites were unaffected by excision of *ama1* (**Fig 3A**).

265

266

### 267 **Fig 3. Sporozoite AMA1 is required for efficient infection of mammalian cells**

268 **A.** Quantification of sporozoite cell traversal activity (% of dextran-positive cells) in rapamycin-  
269 treated *ama1Con* and *ama1cKO* parasites. The values for rapamycin-treated *ama1cKO*  
270 parasites are represented as percentage of the rapamycin-treated *ama1Con* parasites (mean  
271 +/- SEM of three independent experiments). Each data point is the mean of five technical

272 replicates. Ns, non-significant (Two-tailed ratio paired t test). **B.** Quantification of EEFs  
273 development *in vitro*, done by flow cytometry or microscopy analysis of HepG2 cells infected  
274 with sporozoites isolated from either untreated or rapamycin-treated *ama1Con* and *ama1cKO*  
275 infected mosquitoes. The data for rapamycin-treated *ama1Con* and *ama1cKO* parasites are  
276 represented as percentage of the respective untreated parasites (mean +/- SEM). Each data  
277 point is the mean of three technical replicates in one experiment. Ns, non-significant; \*,  $p <$   
278 0.05 (Two-tailed ratio paired t test). **C.** Quantification of excised (mCherry<sup>+</sup>/GFP<sup>-</sup>, red) and non-  
279 excised (mCherry<sup>+</sup>/GFP<sup>+</sup>, green) EEF populations for untreated and treated *ama1Con* and  
280 *ama1cKO* parasites. **D.** Fluorescence microscopy of EEF development (24h p.i.) *in vitro*, in  
281 HepG2 cells infected with salivary gland sporozoites from untreated or rapamycin-treated  
282 *ama1Con* and *ama1cKO* parasites. The right panels show Hoechst (blue), mCherry (red) and  
283 GFP (green) merged images. Scale bar = 10  $\mu$ m. **E.** Immunofluorescence imaging of  
284 mCherry<sup>+</sup>/GFP<sup>-</sup> (excised) rapamycin-treated *ama1Con* and *ama1cKO* EEFs after staining with  
285 anti-UIS4 antibodies (green). The right panels show Hoechst (blue), mCherry (red) and UIS4  
286 (green) merged images. Scale bar = 10  $\mu$ m.

287

288

289 We then infected HepG2 cell cultures with sporozoites isolated from the salivary glands  
290 of mosquitoes previously fed with rapamycin-treated or untreated *ama1Con* and *ama1cKO*  
291 parasites. We quantified infected cells, containing exo-erythrocytic forms (EEFs), at 24 h post  
292 infection by flow cytometry and fluorescence microscopy. We observed a minor but non-  
293 significant reduction in the number of EEFs for rapamycin-treated *ama1Con* parasites  
294 compared to untreated controls (**Fig 3B**). In contrast, the number of EEFs obtained from  
295 hepatocytes infected with rapamycin-treated *ama1cKO* sporozoites was significantly reduced  
296 as compared to untreated parasites (**Fig 3B**). As expected, non-excised (mCherry<sup>+</sup>/GFP<sup>+</sup>)  
297 parasites comprised the majority of EEFs quantified for *ama1Con* and *ama1cKO* untreated  
298 parasites (**Fig 3C**). Conversely, excised (mCherry<sup>+</sup>/GFP<sup>-</sup>) EEFs were predominantly observed  
299 in hepatocytes infected with rapamycin-treated *ama1Con* and *ama1cKO* parasites. However,

300 a small enrichment of non-excised (mCherry<sup>+</sup>/GFP<sup>+</sup>) EEFs was observed with rapamycin-  
301 treated *ama1cKO* (**Fig 3C**), as observed with salivary gland sporozoites (**Fig 2G**). Importantly,  
302 we could not observe any obvious defect in developmental size or morphology in 24h EEFs  
303 between treatment conditions with the two parasite lines, by fluorescence microscopy (**Fig 3D**).  
304 Finally, UIS4 staining of the PV membrane confirmed that mCherry<sup>+</sup>/GFP<sup>-</sup> excised *ama1cKO*  
305 sporozoites could form a PV *in vitro*, similar to EEFs from rapamycin-treated *ama1Con* (**Fig**  
306 **3E**), implying that in the absence of AMA1, sporozoites conserve a residual capacity to  
307 productively invade host cells.

308

### 309 **RON2 and RON4 interact with AMA1 in sporozoites and are required for host cell** 310 **invasion**

311 Merozoite AMA1 interacts with RON proteins for invasion of erythrocytes [21–23]. In  
312 order to investigate whether similar protein interactions also occur in sporozoites, we  
313 performed immunoprecipitation experiments using lysates from transgenic sporozoites  
314 expressing RON4 fused to mCherry and beads coupled to anti-red fluorescent protein (RFP)  
315 nanobodies (RFP-trap). RON4, RON2, RON5 and AMA1 were the main proteins identified by  
316 mass spectrometry among co-precipitated proteins, showing that AMA1-RON interactions are  
317 conserved in salivary gland sporozoites (**S1 Table**). We decided to focus on RON2 and RON4  
318 and generated conditional mutants, using a two-step strategy to introduce LoxN sites upstream  
319 and downstream of the genes in PbDiCre parasites (**Figs 4A, S7 and S8**). Clonal populations  
320 of *ron2cKO* and *ron4cKO* parasites were obtained after pyrimethamine selection and FACS  
321 sorting, and verified by genotyping PCR (**S7 and S8 Figs**). In agreement with an essential role  
322 for RON2 and RON4 in the blood, rapamycin-induced gene excision reduced blood-stage  
323 growth in *ron2cKO* and *ron4cKO* infected mice (**Figs 4B and 4C**).

324

325

326 **Fig 4. RON2 and RON4 are required for sporozoite invasion in the mosquito and**  
327 **mammalian hosts**

328 **A.** Strategy to generate *ron2cKO* and *ron4cKO* parasites in the PbDiCre line. **B-C.** Blood stage  
329 growth of rapamycin-treated and untreated *ron2cKO* (B) and *ron4cKO* (C) parasites. The graph  
330 represents the parasitaemia (mean +/- SEM) in groups of 5 mice. Rapamycin was administered  
331 at day 1. \*\*,  $p < 0.01$ ; \*\*\*\*,  $p < 0.0001$  (Two-way ANOVA). **D-F.** Quantification of midgut  
332 sporozoites (MG-SPZ, D), haemolymph sporozoites (HL-SPZ, E) or salivary gland sporozoites  
333 (SG-SPZ, F) isolated from mosquitoes infected with untreated or rapamycin treated *ron2cKO*  
334 or *ron4cKO* parasites. The graphs show the number of sporozoites per infected female  
335 mosquito (mean +/- SEM). Each dot represents the mean value obtained in independent  
336 experiments after dissection of 30-50 mosquitoes (MG, HL) or 50-70 mosquitoes (SG),  
337 respectively. Ns, non-significant; \*,  $p < 0.05$ ; \*\*,  $p < 0.01$  (Two-tailed ratio paired t test). **G-I.**  
338 Quantification of excised (mCherry<sup>+</sup>/GFP<sup>-</sup>, red) and non-excised (mCherry<sup>+</sup>/GFP<sup>+</sup>, green)  
339 midgut sporozoites (MG-SPZ, G), haemolymph sporozoites (HL-SPZ, H) or salivary gland  
340 sporozoites (SG-SPZ, I) isolated from mosquitoes infected with untreated or rapamycin-treated  
341 *ron2cKO* and *ron4cKO* parasites. **J.** Quantification of EEFs development *in vitro*, done by  
342 microscopy analysis of HepG2 cells infected with sporozoites isolated from either untreated or  
343 rapamycin-treated *ron2cKO* and *ron4cKO* infected mosquitoes. The data for rapamycin-  
344 treated parasites are represented as percentage of the respective untreated parasites (mean  
345 +/- SEM). Each data point is the mean of five technical replicates in one experiment. Ns, non-  
346 significant; \*,  $p < 0.05$  (Two-tailed ratio paired t test). **K.** Quantification of sporozoite cell  
347 traversal activity (% of dextran-positive cells) in untreated and rapamycin-treated *ron2cKO* and  
348 *ron4cKO* parasites. The data for rapamycin-treated parasites are represented as percentage  
349 of the respective untreated parasites (mean +/- SEM). Each data point is the mean of five  
350 technical replicates from one experiment.

351

352

353 We then transmitted *ron2cKO* and *ron4cKO* parasites to mosquitoes, with or without  
354 rapamycin treatment. Both parasite lines could colonize the midgut of mosquitoes as  
355 evidenced by microscopy imaging of midgut oocysts (**S9 Fig**). Rapamycin treatment of

356 *ron2cKO* and *ron4cKO* parasites before transmission led to a modest reduction of midgut and  
357 haemolymph sporozoite numbers (**Figs 4D** and **4E**). However, there was no difference in the  
358 percentage of mosquitoes displaying mCherry-labelled pericardial cells (**S10 Fig**), indicating  
359 no defect in egress from oocysts for both *ron2cKO*<sup>rapa</sup> and *ron4cKO*<sup>rapa</sup> sporozoites. In contrast,  
360 the numbers of salivary gland sporozoites were severely reduced for rapamycin-treated  
361 *ron2cKO* and *ron4cKO* parasites (**Fig 4F**), as observed with the *ama1cKO* line (**Fig 2D**). As  
362 expected, rapamycin treatment before transmission induced robust gene excision in both  
363 *ron2cKO* and *ron4cKO* sporozoites (**Figs 4G-4I**). Despite reduced invasion after rapamycin  
364 treatment we could recover sufficient numbers of *ron2cKO* and *ron4cKO* salivary gland  
365 sporozoites to assess host cell invasion *in vitro*. As observed with *ama1cKO* parasites,  
366 rapamycin-induced gene excision of *ron2* and *ron4* impaired invasion of HepG2 cells, as  
367 shown by reduced EEF numbers (**Fig 4J**). As observed for AMA1-deficient sporozoites, cell  
368 traversal activity was preserved in *ron2cKO* and *ron4cKO* sporozoites after rapamycin  
369 treatment (**Fig 4K**). Overall, our data support an active role for RON2 and RON4 in invasion  
370 of both mosquito salivary glands and hepatocytes, similar to AMA1.

371

### 372 **AMA1 and RON2 play a role at the entry site during invasion of mosquito salivary glands**

373 In order to get more insights into the colonization of the mosquito salivary glands by  
374 sporozoites, we used serial block face-scanning electron microscopy (SBF-SEM) for three-  
375 dimensional volume imaging of whole infected salivary glands. We first compared mosquitoes  
376 infected with WT (PbGFP) or rapamycin-treated *ama1cKO* parasites at day 21 post-feeding.  
377 SBF-SEM data confirmed the lower parasite density in glands infected with *ama1cKO* as  
378 compared to WT (**S11 Fig**). WT sporozoites were observed inside acinar cells and in the apical  
379 secretory cavities, where they clustered in bundles (**S11A Fig** and **Movie 1**). Despite reduced  
380 numbers of sporozoites, we observed a similar distribution of *ama1cKO* parasites inside the  
381 salivary glands, with both intracellular and intraluminal sporozoites (**S11B Fig** and **Movie 2**).  
382 Most of the sporozoites were found lying in direct contact with the cytosol inside acinar cells,  
383 without any visible vacuolar membrane (**S11 and S12 Figs**). Nevertheless, we also observed



384 some sporozoites surrounded by membranes (**S12 Fig**). However, careful examination of the  
385 3D SBF-SEM images revealed that these structures may correspond to invaginations of  
386 cellular membranes surrounding portions of intracellular sporozoites, rather than actual  
387 vacuoles (**S12A-B Figs** and **Movie 3**). Similar to the WT, *ama1*ckO parasites surrounded by  
388 membranes were found inside acinar cells (**S12C Fig**). We also observed sporozoites present  
389 in the secretory cavity and surrounded by a cellular membrane, with both WT (**S12D Fig**) and  
390 *ama1*ckO parasites (**S12E Fig**). These data thus confirmed the defect of colonization of the  
391 mosquito salivary glands by AMA1-deficient sporozoites, but showed no difference in the  
392 distribution of the parasites inside the infected glands or in transcellular migration toward the  
393 secretory cavities, suggesting a defect at the entry step.

394 In an effort to capture sporozoite invasion events we analyzed infected salivary glands  
395 by SBF-SEM at an earlier time point, 15 days post-feeding (**Fig 5**). We were able to visualize  
396 three invasion events with untreated *ama1*ckO parasites (noted as wt) (**Figs 5A-F, S13**, and  
397 **Movie 4**). The extracellular portion of all three sporozoites was lying underneath the basal  
398 lamina (**Figs 5A** and **S13A-B**), tightly adhering to the acinar cell surface throughout the  
399 parasite length (**Figs 5D-E** and **S13E-G**). In all three events, the entry site consisted in a flat  
400 ring-like aperture in the host cell membrane, through which sporozoites were apparently  
401 penetrating smoothly without any major alteration of their shape (**Figs 5C-D** and **S13E-H**). The  
402 circular aperture was tilted from the cell surface plane, so sporozoites appeared to penetrate  
403 the cells tangentially (**Figs S13D-E** and **S13J-K**). Although the resolution was not sufficient to  
404 distinguish all the cellular membranes in detail, the intracellular portion of the invading  
405 sporozoites appeared to be surrounded by a vacuole (**Figs 5A-B** and **S13**). Full rhoptries, as  
406 evidenced by dense material, as well as empty vesicles, suggestive of discharged rhoptries,  
407 were observed at the apical tip of invading parasites (**Figs 5B-C, S13J-K** and **Movie 5**). We  
408 could also find fully internalized sporozoites containing seemingly full and empty rhoptries  
409 (**S14A-B Fig**). Altogether these observations strongly support that sporozoite entry into acinar  
410 cells is associated with rhoptry discharge and the formation of a vacuole.

411

412  
413  
414  
415  
416  
417  
418  
419  
420  
421  
422  
423  
424  
425  
426  
427  
428  
429  
430  
431  
432  
433  
434  
435  
436  
437  
438  
439

**Fig 5. Capturing sporozoite entry into salivary glands with serial block face-scanning electron microscopy (SBF-SEM)**

**A-F.** SBF-SEM images showing an untreated *ama1cKO* sporozoite (noted as wt) penetrating into a mosquito salivary gland cell. Panels A and B show the same parasite in two different sections. In A, the sporozoite is cut twice (black arrows), with one part located outside the cell, underneath the basal lamina (BL, white arrow), and the other one inside the cell, within a vacuole surrounded by a membrane (white arrowhead). In B, a tight vacuole can be seen surrounding the intracellular portion of the invading sporozoite (arrowhead), as well as a full rhoptry (white arrow). The volume segmentation in C shows full rhoptries (blue) and empty vesicles (green) in the apical portion of the parasite. In D, the extracellular and intracellular parts of the sporozoite are colored in purple and pink, respectively, while the cell appears is yellow. The volume image in E shows the host cell surface (yellow), revealing a deep imprint of the extracellular parasite segment (black arrow) and the circular aperture at the point of entry (black arrowhead). In F, the entry site is shown at higher magnification. An overview of the segmentation process corresponding to panels A-F is shown in Movie 4. Segmentation of the rhoptries is shown in Movie 5. **G-K.** SBF-SEM images showing a rapamycin-treated *ron2cKO* sporozoite penetrating into a mosquito salivary gland cell. In G, the sporozoite is caught in the process of entry through an elevated host cell structure (arrow) associated with a tight constriction of the parasite body. The intracellular portion of the parasite is surrounded by a vacuole (white arrowhead). A volume segmentation of the sporozoite is shown in H, superimposed on the same section as in G. In the volume representations in I and J, the extracellular and intracellular parts of the sporozoite are colored in purple and pink, respectively, while the cell appears is yellow. The entry site is marked with an arrowhead, and shown at higher magnification in K. An overview of the segmentation process corresponding to panels G-K is shown in Movie 6. Scale bars, 2  $\mu\text{m}$ .

440 We also captured four invasion events with rapamycin-treated *ron2cKO* parasites (**Figs**  
441 **5G-K, S15 and Movie 6**), revealing several notable differences as compared to control  
442 sporozoites. The entry site consisted in an elevated cup-like structure, with host cell membrane  
443 ruffling and protrusions surrounding the invading parasites (**Figs 5G-K and S15E-J**). Strikingly,  
444 all four mutant sporozoites displayed a marked constriction at the entry point (**Figs 5G-I, S15A-**  
445 **C and S15G-H**). We also noted differences in the parasite positioning as regard to the host  
446 cell surface. While the extracellular portion of control parasites was intimately associated with  
447 the host cell surface (**Figs 5D-E and S13E-G**), mutant sporozoites were captured in a more  
448 upward position, with no adhesion of the parasite rear end to the salivary gland surface (**Figs**  
449 **5G, S15B and S15G-H**). Most of the sporozoite body was internalized, with only a minor portion  
450 localized outside the cell, the junction between the two regions being pinched by host cell  
451 membrane structures (**Figs 5I, S15B-C and S15H**). As seen with control parasites, the  
452 intracellular sporozoite portion was surrounded by a vacuole, which however was wider than  
453 the one seen with WT parasites (**Figs 5G and S15A,D,G**). Also, we observed internalized  
454 RON2-deficient sporozoites containing both full and seemingly empty rhoptries (**S14C and**  
455 **S15D Figs**), indicating that the lack of RON2 does not impair rhoptry discharge. Although we  
456 did not capture invading AMA1-deficient sporozoites, we could find intracellular sporozoites  
457 displaying strong bending of their body (**S16A Fig**), similar to RON2 mutant parasites (**S16B**  
458 **Fig**), possibly caused by a tight constriction inflicted during entry through a dysfunctional  
459 junction. These observations strongly suggest that, in the absence of a functional AMA1-RON  
460 complex, sporozoites are impaired during the invasion process.

461

#### 462 **Invasion by AMA1- or RON2-deficient sporozoites is associated with a loss of integrity** 463 **of the salivary gland epithelium**

464 Interestingly, passage of WT sporozoites from acinar cells to the secretory cavities could  
465 be associated with an alteration of the apical cellular membrane integrity, with leakage of  
466 cytoplasmic material in the secretory cavity (**S17A Fig**). However, the overall architecture of  
467 the infected gland did not seem to be altered despite the presence of numerous sporozoites

468 **(Fig 6A)**. In contrast, salivary glands from mosquitoes infected with rapamycin-treated  
469 *ama1cKO* parasites, despite low parasite loads, showed signs of epithelial damage, with  
470 alteration of the basal membrane and cellular vacuolization **(Fig 6B)**. Closer examination of  
471 SBF-SEM data revealed sites where the basal lamina was ruptured and detached from the  
472 underlying epithelium **(Fig 6C)**. Of note, the basal lamina was not visible in either of the  
473 *ron2cKO* invasion events **(Figs 5 and S15)**, possibly as a result of a complete rupture or  
474 detachment at the entry site. AMA1-deficient sporozoites found close to the surface,  
475 presumably caught shortly after invasion, were sometimes observed inside large vacuoles **(Fig**  
476 **6D)**. In some instances, such large vacuoles were associated with a rupture of the cell plasma  
477 membrane **(Fig 6E)**. Similar cellular damage was also observed with *ron2cKO* mutants **(Fig**  
478 **6F)**.

479

480

481 **Fig 6. Invasion by AMA1- and RON2-deficient sporozoites is associated with a loss of**  
482 **integrity of the mosquito salivary gland epithelium**

483 **A-B.** SBF-SEM sections of salivary glands infected with WT (A) or rapamycin-treated  
484 *ama1cKO* parasites (B), day 21 post-infection. The *ama1cKO*-infected gland shows signs of  
485 cellular damage (black arrows) despite low parasite density. A single intracellular sporozoite  
486 is indicated by a white arrow. Scale bars, 10  $\mu\text{m}$ . **C-E.** SBF-SEM sections of salivary glands  
487 infected with rapamycin-treated *ama1cKO* parasites, day 15 post-infection. Disruption of the  
488 basal lamina is indicated by an arrow. In D, a large vacuole is visible around an intracellular  
489 sporozoite and is indicated by an asterisk. In E, both the basal lamina and the cell plasma  
490 membrane are ruptured (arrow), resulting in a large cellular vacuole that communicates with  
491 the outside (asterisk). Scale bars, 2  $\mu\text{m}$ . **F.** SBF-SEM sections of salivary glands infected with  
492 rapamycin-treated *ron2cKO* parasites, day 15 post-infection. A large vacuole surrounding an  
493 intracellular sporozoite is indicated by an arrow. Scale bar, 2  $\mu\text{m}$ . **G.** Fluorescence microscopy  
494 images of salivary glands infected with untreated (UT) or rapamycin-treated (+Rapa)  
495 *ama1cKO* or *ron2cKO* parasites, day 16 post-infection. Samples were stained with Hoechst

496 77742 (Blue). The panels show mCherry (red), GFP (green) and Hoechst (blue) and  
497 transmitted light merge images. Zones of retraction of the acinar epithelial cells are visible in  
498 the lobes infected with AMA1- and RON2-deficient sporozoites (arrows). Scale bars, 50  $\mu\text{m}$ .  
499 **H.** Quantification of salivary gland lobes showing retracted epithelium after infection with  
500 untreated or rapamycin-treated *ama1cKO* and *ron2cKO* parasites. The data shown are from  
501 two independent experiments (Fisher's exact test,  $P = 0.0286$  for *ama1cKO* and  $P < 0.0001$  for  
502 *ron2cKO*).

503

504

505 To corroborate SBF-SEM observations, we imaged entire salivary glands by  
506 fluorescence microscopy (**Figs 6G** and **S18**). Upon examination of salivary glands infected  
507 with rapamycin-treated *ama1cKO* or *ron2cKO*, we frequently observed zones where epithelial  
508 cells were detached from the basal lamina and retracted, creating pockets suggestive of liquid  
509 accumulation (**Fig 6G**). Such lesions were also observed in salivary glands collected from  
510 mosquitoes fed with untreated *ama1cKO* or *ron2cKO*, albeit at significantly lower frequencies  
511 despite much higher parasite loads (**Fig 6H**). However, heavily infected lobes showed signs of  
512 internal remodeling of the actin cytoskeleton (**S17B Fig**), and were prone to rupture during  
513 manipulation.

514 Collectively, our data support a role of AMA1 and RONs during sporozoite entry into  
515 mosquito acinar cells through a junction, leading to the formation of a transient vacuole.  
516 Dysfunction of the junction in the absence of the AMA1-RON complex impairs parasite entry  
517 and may cause collateral host cell damage.

518

519

## 520 Discussion

521 AMA1 and RON proteins play an essential role in *Plasmodium* merozoites during  
522 invasion of erythrocytes, where they participate in the formation of the MJ. In contrast, their  
523 role in sporozoites was unclear so far. In this study, we exploited the DiCre recombinase  
524 system to delete *ama1*, *ron2* or *ron4* genes in *P. berghei* prior to transmission to mosquitoes,  
525 allowing subsequent functional investigations in sporozoites. We generated *ama1cKO*,  
526 *ron2cKO* and *ron4cKO* parasites in a two-step approach by introducing Lox sites upstream  
527 and downstream of the genes in mCherry-expressing PbDiCre parasites, together with a GFP  
528 cassette to facilitate monitoring of gene excision. Rapamycin treatment of *ama1cKO*, *ron2cKO*  
529 and *ron4cKO* parasites led to a major impairment in blood-stage growth, consistent with an  
530 essential role for AMA1 and RONS in RBC invasion, but without affecting transmission to  
531 mosquitoes. Remarkably, with all three conditional lines, we observed a dramatic (>10-fold)  
532 reduction in the number of salivary gland sporozoites with rapamycin-exposed parasites as  
533 compared to untreated parasites, despite comparable midgut and haemolymph sporozoite  
534 numbers, showing that AMA1 and RONS are important for efficient invasion of the salivary  
535 glands, but not egress from oocysts. AMA1- and RON-deficient sporozoites also displayed a  
536 3-6 fold reduction of invasion of mammalian hepatocytes. The similar phenotype of *ama1cKO*,  
537 *ron2cKO* and *ron4cKO* mutants, combined with mass spectrometry evidence of an interaction  
538 between AMA1 and RON proteins, is consistent with AMA1 playing a role together with the  
539 RON proteins during sporozoite host cell invasion. It thus appears that the function of AMA1  
540 and RONS cannot be dissociated, unlike previously thought [7]. Our data are in line with those  
541 from two studies where a promoter exchange strategy was used to knockdown *ron2*, *ron4* and  
542 *ron5* in *P. berghei* sporozoites [14,15]. All three mutants shared a similar phenotype, with a  
543 defect in salivary gland invasion and reduced infection of HepG2 cell cultures.

544 Our results differ from those of Giovannini *et al.*, who depleted AMA1 in *P. berghei*  
545 sporozoites by targeting the 3'UTR of *ama1* gene using the FLP/FRT conditional system, and  
546 observed no effect during mosquito or hepatocyte infection [7]. In this system, the FLP is under  
547 the control of the *trap* promoter and mediates DNA excision during sporozoite development,

548 resulting in late depletion of AMA1 protein (beyond day 16 post-feeding), a time frame that  
549 would not permit the observation of a salivary gland invasion phenotype. In contrast, with the  
550 DiCre system as used here, excision occurs in blood stages prior to transmission to  
551 mosquitoes, long before sporozoites are formed and produce AMA1 and RON proteins. The  
552 presence of residual AMA1 protein in salivary gland sporozoites after FLP-mediated excision  
553 of the 3'UTR could also explain why no defect in hepatocyte invasion was observed in the  
554 previous study. Deletion of the 3'UTR of *ama1* using the DiCre system was not sufficient to  
555 abrogate protein expression in our study, as reported before with other genes in *P. berghei*  
556 and *P. falciparum* [17,24]. In the *ama1* $\Delta$ utr line, the downstream genomic sequence (used as  
557 a 3' homology region) may be sufficient to stabilize the transcripts and compensate for the lack  
558 of 3'UTR following rapamycin-induced excision. This could also contribute to the discrepancy  
559 between our results and the previous report by Giovannini *et al.*, where upon recombination  
560 the 3'UTR was replaced by a plasmid backbone sequence [7].

561 Invasion of salivary glands by *Plasmodium* sporozoites remains a poorly characterized  
562 process. A previous electron microscopy analysis of the salivary glands of *Aedes aegypti*  
563 mosquitoes infected with avian *P. gallinaceum* documented sporozoites entering the salivary  
564 glands through an invagination of the basal lamina while forming a junctional area between  
565 the anterior tip of the sporozoite and the plasma membrane of the acinar cells [25]. The same  
566 study showed that newly invaded sporozoites were surrounded by a vacuole inside acinar  
567 cells, while those that had entered the secretory cavities were either devoid of a vacuole or  
568 present inside disintegrating vacuoles [25]. In another study, *P. falciparum* sporozoites were  
569 observed penetrating salivary glands of *Anopheles stephensi* mosquitoes through holes in the  
570 basal membrane without causing any obvious damage to the gland [26]. Here, using three-  
571 dimensional volume electron microscopy, we could capture *P. berghei* sporozoites in the  
572 process of entering acinar cells in *A. stephensi* mosquitoes. Our data support that haemolymph  
573 sporozoites initially enter the salivary glands by forming a transient vacuole. During traversal  
574 of mammalian cells, sporozoites use the perforin-like protein 1 (PLP1) to egress from transient  
575 vacuoles [27]. Whether sporozoites use a similar machinery to exit the entry vacuole in the

576 mosquito salivary glands remains to be determined. Imaging of three invasion events with  
577 control parasites showed sporozoites intimately adhering to the cell surface and penetrating  
578 inside a nascent vacuole through a ring-like aperture, suggestive of a MJ. All three invading  
579 WT sporozoites were located between the basal lamina and the epithelial cells. How  
580 sporozoites cross the basal lamina remains unclear, but might involve the secretion of parasite  
581 proteases. Our functional data combined with the SBF-SEM images suggest that RONS are  
582 secreted from rhoptries prior to or during invasion of the salivary glands, where they could form  
583 a complex with AMA1 at the entry junction. Consistent with a rhoptry discharge event  
584 associated with salivary gland invasion, previous ultrastructural imaging studies of sporozoites  
585 have reported the presence of four or more rhoptries in midgut-derived sporozoites, as  
586 opposed to two in mature salivary gland sporozoites [8,28–30].

587 SBF-SEM also revealed morphological defects at the entry site of RON2-deficient  
588 sporozoites, with intense host cell membrane ruffling associated with a tight constriction of the  
589 parasite body at the entry site. These observations suggest that, despite the absence of a  
590 functional AMA1-RON complex, mutant sporozoites are still capable of forming a junction.  
591 Interestingly, while invading WT sporozoites were adhering to the host cell surface along their  
592 body, the RON2 mutants entered cells in an upward position, as described before with AMA1-  
593 deficient *T. gondii* tachyzoites [7,11]. While we cannot formally exclude a role of AMA1-RONS  
594 in parasite attachment to the host cell, it is possible that blockage of the entry of RON2-deficient  
595 sporozoites resulted in detachment of their rear end from the cell surface. These observations  
596 strongly suggest that RON2-deficient sporozoites were halted during the process of entry  
597 through a dysfunctional junction. Host cell invasion by apicomplexan zoites relies on a  
598 balanced combination between host cell membrane dynamics and parasite motor function [32].  
599 The membrane ruffling surrounding invading RON2-deficient sporozoites is reminiscent of  
600 actin-driven host cell protrusions observed with myosin A-deficient *T. gondii* tachyzoites, which  
601 are impaired during entry due to a motility defect [33]. Beyond participating in the assembly of  
602 the junction, AMA1 and RONS could be required to ensure proper function of the junction



603 during invasion of mosquito acinar cells, possibly through interactions with host cell  
604 cytoskeleton components as described with RONs in *T. gondii* [31].

605 Interestingly, infection of the mosquito salivary glands by AMA1- or RON2-deficient  
606 sporozoites was associated with a loss of integrity of the epithelium, with rupture of the basal  
607 lamina and cell vacuolization. This suggests that during sporozoite entry into the salivary gland,  
608 AMA1-RONs may contribute to maintaining a sealed junction around the parasite, to allow  
609 invasion without creating a leak, thus preventing cell damage. In line with this hypothesis,  
610 erythrocyte lysis has been observed during invasion of AMA1-depleted *P. falciparum*  
611 merozoites [34]. Our data thus provide a possible molecular basis to explain how thousands  
612 of sporozoites can colonize the salivary glands of a single mosquito without causing overt  
613 tissue damage. As sporozoites can remain in the salivary cavities for several days before they  
614 are transmitted, harmless entry in the glands is likely essential to ensure parasite transmission.  
615 Damage inflicted to the salivary gland epithelium during invasion of AMA1-RON mutants may  
616 also have detrimental effects on mosquito feeding and survival.

617 Despite the significant reduction in numbers, a minor proportion of rapamycin-treated  
618 *ama1cKO*, *ron2cKO* and *ron4cKO* sporozoites could still invade the salivary glands of infected  
619 mosquitoes. While we cannot exclude the presence of residual non-excised parasites inside  
620 infected glands in the SFB-SEM experiments, these parasites should only represent a minority  
621 of salivary gland sporozoites after rapamycin exposure (<10%). Some mutant parasites may  
622 succeed in penetrating the glands despite a dysfunctional junction, as suggested by our SFB-  
623 SEM data. Alternatively, some degree of plasticity may allow sporozoites to use alternative  
624 adhesion or invasion ligands, as observed in *T. gondii* where paralogs can compensate for the  
625 lack of a functional AMA1-RON2 pair [35]. While there is no known paralog of RON2 in  
626 *Plasmodium*, the Membrane Associated Erythrocyte Binding-Like protein (MAEBL) contains  
627 two AMA1-like domains [36], and was in fact reported to be essential for invasion of the salivary  
628 glands [37,38]. Interestingly, MAEBL was not identified by co-immunoprecipitation in the  
629 RON2, RON4, RON5 complex in oocyst [15] or salivary gland (this study) derived sporozoites,

630 and AMA1-deficient sporozoites fail to invade the mosquito salivary glands, thus arguing  
631 against a compensatory role for MAEBL in AMA1-deficient sporozoites.

632 When tested on hepatocyte cell cultures, only a minor proportion of AMA1, RON2 or  
633 RON4-depleted salivary gland sporozoites productively invaded and developed into EEFs. The  
634 defect in hepatocyte invasion was less pronounced in comparison to that observed for the  
635 salivary glands. This differential dependency on AMA1-RONs during host cell invasion could  
636 relate to different membrane properties impacting the junction [32]. Consistent with our results,  
637 a previous study has shown that anti-AMA1 only partially inhibited *P. falciparum* infection of  
638 human hepatocytes *in vitro* [4]. Interestingly, knockdown of RON2 in sporozoites was shown  
639 to affect cell traversal and hepatocyte invasion, both *in vitro* and *in vivo*, with the authors  
640 implying that loss of RON2 affected attachment to both the salivary glands and hepatocytes,  
641 thereby influencing invasion [14]. An earlier report on *P. falciparum* sporozoites showed that  
642 interfering with the AMA1-RON2 interaction affected host cell traversal [13]. However, in our  
643 study, rapamycin-treated *ama1cKO*, *ron2cKO* and *ron4cKO* parasites showed no defect in  
644 sporozoite cell traversal but were impaired in productive invasion. While these differences in  
645 phenotypes could be attributed to differences between *P. falciparum* and *P. berghei*, it is  
646 possible that the use of salivary gland sporozoites in our study versus those obtained from the  
647 haemolymph by Ishino *et al.* accounted for the difference in observations for cell traversal  
648 between experiments. We only assessed sporozoite infectivity in HepG2 cell cultures, showing  
649 a 3-6 fold reduction in host cell invasion. It is possible that more severe defects would be  
650 observed under *in vivo* conditions, but the low numbers of AMA1- and RON-deficient  
651 sporozoites recovered from mosquito salivary glands precluded their analysis *in vivo* in mice.

652 Based on our findings, we propose a model where *Plasmodium* sporozoites use the  
653 AMA1-RON complex twice, in the mosquito and mammalian hosts (**Fig 7**). First, AMA1 and  
654 RONs could mediate the safe entry of sporozoites into the salivary glands via the formation of  
655 a junction and a transient vacuole, in a cell-specific manner and without compromising the cell  
656 membrane integrity, to ensure successful colonization of the glands and subsequent parasite  
657 transmission. This model fits with previous reports showing that sporozoites can massively

658 infect salivary glands without causing cellular damage [39,40]. This crossing event would differ  
659 from the cell traversal activity of mature sporozoites in the mammalian host, which is  
660 associated with a loss of membrane integrity and cell death [41]. Following sporozoite  
661 inoculation into the mammalian host, AMA1 and RONs facilitate productive invasion of  
662 hepatocytes, presumably through the formation of a canonical MJ that leads to the formation  
663 of the PV where the parasite can replicate into merozoites. Colonization of the salivary glands  
664 and productive invasion of hepatocytes involve transcellular migration versus establishment of  
665 a replicative vacuole, respectively. However, both events likely require tight membrane sealing  
666 around the invading parasite and subversion of the host cortical cytoskeleton, a function that  
667 could rely on the AMA1-RON complex. Our study reveals that the contribution of AMA1 and  
668 RON proteins is conserved across *Plasmodium* invasive stages. Pre-clinical studies have  
669 shown that vaccination with the AMA1-RON2 complex induces functional antibodies that better  
670 recognize AMA1 as it appears complexed with RON2 during merozoite invasion, providing an  
671 attractive vaccine strategy against *Plasmodium* blood stages [42,43]. Our results indicate that  
672 the AMA1-RON complex might also be considered as a potential target to block malaria  
673 transmission.

674

675

676 **Fig 7. Model of AMA1-RON function in *Plasmodium* sporozoites.** AMA1 and RON proteins  
677 drive two distinct sporozoite invasion events in the mosquito and mammalian hosts. After  
678 egress from oocysts, sporozoites first rely on AMA1 and RONs to enter the mosquito salivary  
679 glands inside a transient vacuole, without causing epithelium damage, to eventually  
680 accumulate in the secretory cavities after crossing the acinar cells. Then, following parasite  
681 transmission to a mammalian host, AMA1 and RONs are required for efficient productive  
682 invasion of hepatocytes inside a parasitophorous vacuole. Both events supposedly involve  
683 rhoptry secretion and the formation of a junction, which however is uncoupled from the  
684 formation of a canonical parasitophorous vacuole during colonization of the insect salivary  
685 glands.

686 **Materials and methods**

687 **Mice**

688 Female Swiss mice (6–8 weeks old, from Janvier Labs) were used for all routine parasite  
689 infections. All animal work was conducted in strict accordance with the Directive 2010/63/EU  
690 of the European Parliament and Council ‘On the protection of animals used for scientific  
691 purposes’. Protocols were approved by the Ethical Committee Charles Darwin N°005  
692 (approval #7475-2016110315516522).

693

694 **Parasites**

695 Conditional genome editing was performed in the *P. berghei* (ANKA strain) PbDiCre line,  
696 obtained after integration of mCherry and DiCre expression cassettes at the dispensable  
697 *p230p* locus [19]. Two additional lines expressing RON4-mCherry (bioRxiv  
698 2021.10.25.465731) and/or GFP [44] were used for immunoprecipitation and electron  
699 microscopy experiments, respectively. Parasites were maintained in mice through  
700 intraperitoneal injections of frozen parasite stocks. *Anopheles stephensi* mosquitoes were  
701 reared at 24°C with 80 % humidity and permitted to feed on infected mice that were  
702 anaesthetized, using standard methods of mosquito infection as previously described [45].  
703 Post feeding, *P. berghei*-infected mosquitoes were kept at 21°C and fed daily on a 10%  
704 sucrose solution.

705

706 **Host cell cultures**

707 HepG2 cells (ATCC HB-8065) were cultured in DMEM supplemented with 10% fetal calf  
708 serum, 1% Penicillin-Streptomycin and 1% L-Glutamine as previously described [46], in culture  
709 dishes coated with rat tail collagen I (Becton-Dickinson).

710

711 **Vector construction**

712 In order to target different genes of interest, we first generated a generic plasmid,  
713 pDownstream1Lox (Addgene #164574), containing a GFP-2A-hDHFR cassette under the

714 control of a *P. yoelii hsp70* promoter and followed by the 3'UTR of *P. berghei calmodulin (cam)*  
715 gene and a single LoxN site. The plasmid also contains a yFCU cassette to enable the  
716 elimination of parasites carrying episomes by negative selection with 5-fluorocytosine.

717 The *ama1Con* plasmid was designed to excise only ~30 bp downstream of *P. berghei ama1*  
718 3'UTR. Two fragments were inserted on each side of the GFP-2A-hDHFR cassette of the  
719 pDownstream1Lox plasmid: a 5' homology region (HR) homologous to the terminal portion of  
720 *ama1* (ORF and 3' UTR) followed by a single LoxN site, and a 3' HR homologous to a  
721 sequence downstream of the 3' UTR of *ama1* gene. The *ama1 $\Delta$ utr* plasmid was assembled  
722 similarly to the *ama1Con* construct except that the 5' HR consisted in the terminal portion of  
723 *ama1* ORF followed by a LoxN site and the 3' UTR of *P. yoelii ama1*, to allow excision of the  
724 3'UTR upon rapamycin activation of DiCre. The *ama1cKO* plasmid was designed to introduce  
725 a single LoxN site upstream of *ama1* in the rapamycin-treated (excised) *ama1Con* parasites,  
726 which already contained a residual LoxN site downstream of the gene. To generate the  
727 *ama1cKO* plasmid, the pDownstream1Lox vector was first modified to remove the downstream  
728 LoxN site. Then, a 5' HR and a 3' HR, both homologous to sequences located upstream of  
729 *ama1* gene, were cloned into the modified plasmid on each side of the GFP-2A-hDHFR, with  
730 a single LoxN site introduced upstream of the GFP-2A-hDHFR cassette.

731 To generate *ron2cKO* and *ron4cKO* constructs, two separate plasmids, P1 and P2, were  
732 generated to insert a LoxN site upstream of the promoter and downstream of the gene of  
733 interest, respectively, in two consecutive transfections. P1 plasmids were constructed by  
734 insertion of 5' and 3' HR on each side of the GFP-2A-hDHFR cassette in the  
735 pDownstream1Lox plasmid, with a second LoxN site introduced upstream of the GFP cassette.  
736 The 5' HR and 3' HR correspond to consecutive fragments located in the promoter region of  
737 the GOI. Because the intergenic sequence between *ron4* gene and its upstream gene is short,  
738 and in order to maintain expression of the upstream gene and exclude any unwanted  
739 duplication and spontaneous recombination events, we introduced the 5' HR of *ron4* in two  
740 fragments, with fragment 1 corresponding to the region just upstream of the ORF while  
741 fragment 2 corresponded to the 3' UTR from the *P. yoelii* ortholog of the upstream gene. P2

742 plasmids were constructed in a similar manner by insertion of a 5' HR and a 3'HR on each side  
743 of the GFP-2A-hDHFR cassette in the pDownstream1Lox plasmid. The 3' HR regions  
744 corresponded to the 3' UTR sequences of *RON2* or *RON4*, respectively. For both target genes,  
745 the 5' HR was divided into two fragments, where fragment 1 corresponded to the end of the  
746 ORF followed by a triple Flag tag, and fragment 2 corresponded to the 3' UTR from the *P.*  
747 *yoelii* ortholog gene, in order to avoid duplication of the 3' UTR region and spontaneous  
748 recombination.

749 All plasmid inserts were amplified by PCR using standard PCR conditions and the CloneAmp  
750 HiFi PCR premix (Takara). Following a PCR purification step (QIAquick PCR purification kit),  
751 the fragments were sequentially ligated into the target vector using the In-Fusion HD Cloning  
752 Kit (Clontech). The resulting plasmid sequences were verified by Sanger sequencing (GATC  
753 Biotech) and linearized before transfection. All the primers used for plasmid assembly are  
754 listed in **Table S2**.

755

## 756 **Parasite transfection**

757 For parasite transfection, schizonts purified from an overnight culture of PbDiCre parasites  
758 were transfected with 5–10 µg of linearized plasmid by electroporation using the AMAXA  
759 Nucleofector device (Lonza, program U033), as previously described [47], and immediately  
760 injected intravenously into the tail vein of Swiss mice. For selection of resistant transgenic  
761 parasites, pyrimethamine (35 mg/L) and 5-fluorocytosine (0.5 mg/ml) were added to the drinking  
762 water and administered to mice, one day after transfection. Transfected parasites were sorted  
763 by flow cytometry on a FACSAria II (Becton-Dickinson), as described [44], and cloned by  
764 limiting dilutions and injections into mice. The parasitaemia was monitored daily by flow  
765 cytometry and the mice sacrificed at a parasitaemia of 2-3%. The mice were bled and the  
766 infected blood collected for preparation of frozen stocks (1:1 ratio of fresh blood mixed with  
767 10% Glycerol in Alsever's solution) and isolation of parasites for genomic DNA extraction,  
768 using the DNA Easy Blood and Tissue Kit (Qiagen), according to the manufacturer's  
769 instructions. Specific PCR primers were designed to check for wild-type and recombined loci

770 and are listed in **Table S2**. Genotyping PCR reactions were carried out using Recombinant  
771 Taq DNA Polymerase (5U/μl from Thermo Scientific) and standard PCR cycling conditions.

772

### 773 ***In vivo* analysis of conditional mutants**

774 DiCre recombinase mediated excision of targeted DNA sequences *in vivo* was achieved by a  
775 single oral administration of 200μg rapamycin (1mg/ml stock, Rapamune, Pfizer) to mice.

776 Excision of the GFP cassette in blood stage parasites was monitored by flow cytometry using  
777 a Guava EasyCyte 6/2L bench cytometer equipped with 488 nm and 532 nm lasers (Millipore)

778 to detect GFP and mCherry, respectively. To analyze parasite development in the mosquito,

779 rapamycin was administered to infected mice 24 hours prior to transmission to mosquitoes, as

780 described [19]. Midguts were dissected out at day 14 post infection. The haemolymph was

781 collected by flushing the haemocoel with complete DMEM, day 14 to 16 post infection. Salivary

782 gland sporozoites were collected between 21–28 days post feeding from infected mosquitoes,

783 by hand dissection and homogenization of isolated salivary glands in complete DMEM. Live

784 samples (infected mosquito midguts or salivary glands, sporozoites) were mounted in PBS

785 and visualized live using a Zeiss Axio Observer.Z1 fluorescence microscope equipped with a

786 LD Plan-Neofluar 403/0.6 Corr Ph2 M27 objective. The exposure time was set according to

787 the positive control and maintained for both untreated and rapamycin-treated parasites, in

788 order to allow comparisons. All images were processed with ImageJ for adjustment of contrast.

789

### 790 ***In vitro* sporozoite assays**

791 HepG2 cells were seeded at a density of 30,000 cells/well in a 96-well plate for flow cytometry

792 analysis or 100,000 cells/well in 8 well μ-slide (IBIDI) for immunofluorescence assays, 24 hours

793 prior to infection with sporozoites. On the day of the infection, the culture medium in the wells

794 was discarded and fresh complete DMEM was added along with 10,000 sporozoites, followed

795 by incubation for 3 hours at 37°C. After 3 hours, the wells were washed twice with complete

796 DMEM and then incubated for another 24-48 hours at 37°C and 5% CO<sub>2</sub>. For quantification of

797 EEF numbers, the cells were trypsinized after two washes with PBS, followed by addition of

798 complete DMEM and one round of centrifugation at 4°C. After discarding the supernatant, the  
799 cells were either directly re-suspended in complete DMEM for flow cytometry, or fixed with 2%  
800 PFA for 10 minutes, subsequently washed once with PBS and then re-suspended in PBS for  
801 FACS acquisition. For quantification of traversal events, fluorescein-conjugated dextran  
802 (0.5mg/ml, Life Technologies) was added to the wells along with sporozoites followed by an  
803 incubation at 37°C for 3 hours. After 3 hours, the cells were washed twice with PBS, trypsinized  
804 and resuspended in complete DMEM for analysis by flow cytometry.

805

### 806 **RON4 immunoprecipitation and mass spectrometry**

807 Freshly dissected RON4-mCherry sporozoites were lysed on ice for 30 min in a lysis buffer  
808 containing 0.5% w/v NP40 and protease inhibitors. After centrifugation (15,000 × g, 15 min,  
809 4°C), supernatants were incubated with protein G-conjugated sepharose for preclearing  
810 overnight. Precleared lysates were subjected to mCherry immunoprecipitation using RFP-Trap  
811 beads (Chromotek) for 2h at 4°C, according to the manufacturer's protocol. PbGFP parasites  
812 with untagged RON4 were used as a control. After washes, proteins on beads were eluted in  
813 2X Laemmli and denatured (95°C, 5min). After centrifugation, supernatants were collected for  
814 further analysis. Samples were subjected to a short SDS-PAGE migration, and gel pieces were  
815 processed for protein trypsin digestion by the DigestProMSi robot (Intavis), as described [10].  
816 Peptide were separated on an Aurora UHPLC column from IonOpticks (25 cm x 75 µm, C18),  
817 using a 30 min gradient from 3 to 32% ACN with 0.1% formic acid, and analyzed on a timsTOF  
818 PRO mass spectrometer (Bruker). Mascot generic files were processed with X!Tandem  
819 pipeline (version 0.2.36) using the PlasmoDB\_PB\_39\_PbergheiANKA database, as described  
820 [10]. The mass spectrometry proteomics data have been deposited to the ProteomeXchange  
821 Consortium via the PRIDE [48] partner repository with the dataset identifier PXD031463.

822

### 823 **Immunofluorescence assays**

824 Blood-stage schizonts were fixed with 4% PFA and 0.0075% glutaraldehyde for 30 mins at  
825 37°C with constant shaking. The samples were then quenched/permeabilized with 125mM



826 glycine /0.1% Triton X-100 for 15 minutes, blocked with PBS/3% BSA, then incubated with Rat  
827 anti-AMA1 antibodies (1:250, clone 28G2, MRA-897A, Bei Resources) followed by Alexa Fluor  
828 goat anti-rat 405 antibodies (1:1000, Life Technologies). The samples were mounted in PBS  
829 and immediately visualized under a fluorescence microscope. Sporozoites were resuspended  
830 in PBS, added on top of poly-L-lysine coated coverslips and allowed to air dry. The sporozoites  
831 were then fixed with 4% PFA for 30 mins, followed by quenching with 0.1M glycine for 30 mins  
832 and two washes with PBS. In the next step, the sporozoites were permeabilized with 1% Triton-  
833 X100 for 5 mins, washed twice with PBS, then blocked with PBS 3%BSA for 1hr at RT and  
834 incubated with anti-AMA1 antibody (1:250) diluted in blocking solution. Following 3 washes  
835 with PBS, the sporozoites were incubated with the secondary antibody (anti-Rat Alexa Fluor  
836 647) diluted in blocking solution. Following 3 washes with PBS, the coverslips were mounted  
837 onto a drop of prolong diamond anti-fade mounting solution (Life Technologies), sealed with  
838 nail polish and imaged using a fluorescence microscope. Infected HepG2 cell cultures were  
839 washed twice with PBS, then fixed with 4% PFA for 20 minutes, followed by two washings with  
840 PBS and incubation with goat anti-UIS4 primary antibody (1:500, Sicgen), followed by donkey  
841 anti-goat Alexa Fluor 594 secondary antibody (1:1000, Life Technologies). For fluorescence  
842 imaging of entire glands, freshly dissected salivary glands were fixed in 4% PFA for 30 minutes  
843 and permeabilized in acetone for 90 seconds, as described [40]. Samples were incubated with  
844 Phalloidin-iFluor 647 (Abcam) and Hoechst 77742 (Life Technologies ) overnight at 4°C,  
845 washed and mounted in PBS before imaging. Acquisitions were made on a Zeiss Axio  
846 Observer Z1 fluorescence microscope using the Zen software (Zeiss). Images were processed  
847 with ImageJ for adjustment of contrast.

848

#### 849 **Serial block face-scanning electron microscopy**

850 For Serial Block Face-Scanning Electron Microscopy (SBF-SEM), salivary glands were  
851 isolated from infected mosquitoes at day 15 or 21 post-feeding, and fixed in 0.1 M cacodylate  
852 buffer containing 3% PFA and 1% glutaraldehyde during 1 hour at room temperature. Intact  
853 salivary glands were then prepared for SBF-SEM (NCMIR protocol) [49] as follows: samples

854 were post-fixed for 1 hour in a reduced osmium solution containing 1% osmium tetroxide, 1.5%  
855 potassium ferrocyanide in PBS, followed by incubation with a 1% thiocarbohydrazide in water  
856 for 20 minutes. Subsequently, samples were stained with 2% OsO<sub>4</sub> in water for 30 minutes,  
857 followed by 1% aqueous uranyl acetate at 4 °C overnight. Samples were then subjected to en  
858 bloc Walton's lead aspartate staining [50], and placed in a 60 °C oven for 30 minutes. Samples  
859 were then dehydrated in graded concentrations of ethanol for 10 minutes in each step. The  
860 samples were infiltrated with 30% agar low viscosity resin (Agar Scientific Ltd, UK) in ethanol,  
861 for 1 hour, 50% resin for 2 hours and 100% resin overnight. The resin was then changed and  
862 the samples were further incubated during 3 hours, prior to inclusion by flat embedding  
863 between two slides of Aclar® and polymerization for 18 hours at 60 °C. The polymerized blocks  
864 were mounted onto aluminum stubs for SBF-SEM imaging (FEI Microtome 8 mm SEM Stub,  
865 Agar Scientific), with two-part conduction silver epoxy kit (EMS, 12642-14). For imaging,  
866 samples on aluminum stubs were trimmed using an ultramicrotome and inserted into a  
867 TeneoVS SEM (ThermoFisher Scientific). Acquisitions were performed with a beam energy of  
868 2 kV, 400 pA current, in LowVac mode at 40 Pa, a dwell time of 1 μs per pixel at 10 nm pixel  
869 size. Sections of 50 nm were serially cut between images. Data acquired by SBF-SEM were  
870 processed using Fiji and Amira (ThermoFisher Scientific). Data alignment and manual  
871 segmentation were performed using Amira.

872

### 873 **Quantification and statistical analysis**

874 *In vitro* experiments were performed with a minimum of three technical replicates per  
875 experiment. Statistical significance was assessed by two-way ANOVA, one-way ANOVA  
876 followed by Tukey's multiple comparisons, Fisher's exact or ratio paired t tests, as indicated in  
877 the figure legends. All statistical tests were computed with GraphPad Prism 5 (GraphPad  
878 Software). The quantitative data used to generate the figures and the statistical analysis are  
879 presented in **Table S3**.

880

### 881 **Acknowledgements**

882 We thank Jean-François Franetich, Maurel Tefit and Thierry Houpert for rearing of mosquitoes,  
883 and Maryse Lebrun for helpful discussions. The following reagent was obtained through BEI  
884 Resources, NIAID, NIH: Monoclonal Anti-*Plasmodium* Apical Membrane Antigen 1, Clone  
885 28G2 (produced *in vitro*), MRA-897A, contributed by Alan W. Thomas. This work was funded  
886 by grants from the Laboratoire d'Excellence ParaFrap (ANR-11-LABX-0024), the Agence  
887 Nationale de la Recherche (ANR-16-CE15-0004 and ANR-16-CE15-0010) and the Fondation  
888 pour la Recherche Médicale (EQU201903007823). The authors acknowledge the Conseil  
889 Régional d'Ile-de-France, Sorbonne Université, the National Institute for Health and Medical  
890 Research (INSERM) and the Biology, Health and Agronomy Infrastructure (IBiSA) for funding  
891 the timsTOF PRO. We acknowledge the ImagoSeine core facility of the Institut Jacques  
892 Monod, member of the France BioImaging infrastructure (ANR-10-INBS-04) and GIS-IBiSA,  
893 and funded by Région Ile-de-France (TeneoVS). ML was supported by a 'DIM 1Health'  
894 doctoral fellowship awarded by the Conseil Régional d'Ile-de-France. AW is supported by the  
895 ATIP-Avenir program.

896

897

898

899 **References**

- 900 1. Besteiro S, Dubremetz JF, Lebrun M. The moving junction of apicomplexan parasites:  
901 A key structure for invasion. *Cell Microbiol.* 2011;13: 797–805. doi:10.1111/j.1462-  
902 5822.2011.01597.x
- 903 2. Cowman AF, Tonkin CJ, Tham W-H, Duraisingh MT. The Molecular Basis of  
904 Erythrocyte Invasion by Malaria Parasites. *Cell Host Microbe.* 2017;22: 232–245.  
905 doi:10.1016/j.chom.2017.07.003
- 906 3. Frénal K, Dubremetz J-F, Lebrun M, Soldati-Favre D. Gliding motility powers invasion  
907 and egress in Apicomplexa. *Nat Rev Microbiol.* 2017;15: 645–660.  
908 doi:10.1038/nrmicro.2017.86
- 909 4. Silvie O, Franetich J-FFJ-F, Charrin S, Mueller MSSMS, Siau A, Bodescot M, et al. A  
910 role for apical membrane antigen 1 during invasion of hepatocytes by *Plasmodium*  
911 *falciparum* sporozoites. *J Biol Chem.* 2004;279: 9490–9496.  
912 doi:10.1074/jbc.M311331200
- 913 5. Tufet-Bayona M, Janse CJ, Khan SM, Waters AP, Sinden RE, Franke-Fayard B.  
914 Localisation and timing of expression of putative *Plasmodium berghei* rhoptry proteins  
915 in merozoites and sporozoites. *Mol Biochem Parasitol.* 2009;166: 22–31.
- 916 6. Lindner SE, Swearingen KE, Harupa A, Vaughan AM, Sinnis P, Moritz RL, et al. Total  
917 and putative surface proteomics of malaria parasite salivary gland sporozoites. *Mol*  
918 *Cell Proteomics.* 2013;12: 1127–1143. doi:10.1074/mcp.M112.024505
- 919 7. Giovannini D, Späth S, Lacroix C, Perazzi A, Bargieri D, Lagal V, et al. Independent  
920 roles of apical membrane antigen 1 and rhoptry neck proteins during host cell invasion  
921 by apicomplexa. *Cell Host Microbe.* 2011;10: 591–602.  
922 doi:10.1016/j.chom.2011.10.012
- 923 8. Tokunaga N, Nozaki M, Tachibana M, Baba M, Matsuoka K, Tsuboi T, et al.  
924 Expression and Localization Profiles of Rhoptry Proteins in *Plasmodium berghei*  
925 Sporozoites. *Front Cell Infect Microbiol.* 2019;9: 316. doi:10.3389/fcimb.2019.00316
- 926 9. Swearingen KE, Lindner SE, Flannery EL, Vaughan AM, Morrison RD, Patrapuvich R,

927 et al. Proteogenomic analysis of the total and surface-exposed proteomes of  
928 *Plasmodium vivax* salivary gland sporozoites. Ribeiro JMC, editor. PLoS Negl Trop  
929 Dis. 2017;11: e0005791. doi:10.1371/journal.pntd.0005791

930 10. Hamada S, Pionneau C, Parizot C, Silvie O, Chardonnet S, Marinach C. In-depth  
931 proteomic analysis of *Plasmodium berghei* sporozoites using trapped ion mobility  
932 spectrometry with parallel accumulation-serial fragmentation. *Proteomics*. 2021;21.  
933 doi:10.1002/pmic.202000305

934 11. Bargieri DY, Andenmatten N, Lagal V, Thiberge S, Whitelaw JA, Tardieux I, et al.  
935 Apical membrane antigen 1 mediates apicomplexan parasite attachment but is  
936 dispensable for host cell invasion. *Nat Commun*. 2013;4: 2552.  
937 doi:10.1038/ncomms3552

938 12. Harris KS, Casey JL, Coley AM, Masciantonio R, Sabo JK, Keizer DW, et al. Binding  
939 hot spot for invasion inhibitory molecules on *Plasmodium falciparum* apical membrane  
940 antigen 1. *Infect Immun*. 2005;73. doi:10.1128/IAI.73.10.6981-6989.2005

941 13. Yang ASP, Lopaticki S, O'Neill MT, Erickson SM, Douglas DN, Kneteman NM, et al.  
942 AMA1 and MAEBL are important for *Plasmodium falciparum* sporozoite infection of the  
943 liver. *Cell Microbiol*. 2017;19: e12745. doi:10.1111/cmi.12745

944 14. Ishino T, Murata E, Tokunaga N, Baba M, Tachibana M, Thongkuiatkul A, et al.  
945 Rhoptry neck protein 2 expressed in *Plasmodium* sporozoites plays a crucial role  
946 during invasion of mosquito salivary glands. *Cell Microbiol*. 2019;21: e12964.  
947 doi:10.1111/cmi.12964

948 15. Nozaki M, Baba M, Tachibana M, Tokunaga N, Torii M, Ishino T. Detection of the  
949 Rhoptry Neck Protein Complex in *Plasmodium* Sporozoites and Its Contribution to  
950 Sporozoite Invasion of Salivary Glands. *mSphere*. 2020;5: e00325-20.  
951 doi:10.1128/msphere.00325-20

952 16. Andenmatten N, Egarter S, Jackson AJ, Jullien N, Herman J-P, Meissner M.  
953 Conditional genome engineering in *Toxoplasma gondii* uncovers alternative invasion  
954 mechanisms. *Nat Methods*. 2012;10: 125–127. doi:10.1038/nmeth.2301

- 955 17. Collins CR, Das S, Wong EH, Andenmatten N, Stallmach R, Hackett F, et al. Robust  
956 inducible Cre recombinase activity in the human malaria parasite *Plasmodium*  
957 *falciparum* enables efficient gene deletion within a single asexual erythrocytic growth  
958 cycle. *Mol Microbiol.* 2013;88: 687–701. doi:10.1111/mmi.12206
- 959 18. Tibúrcio M, Yang ASP, Yahata K, Suárez-Cortés P, Belda H, Baumgarten S, et al. A  
960 Novel Tool for the Generation of Conditional Knockouts To Study Gene Function  
961 across the *Plasmodium falciparum* Life Cycle. *MBio.* 2019;10: e01170-19.  
962 doi:10.1128/mbio.01170-19
- 963 19. Fernandes P, Briquet S, Patarot D, Loubens M, Hoareau-Coudert B, Silvie O. The  
964 dimerisable Cre recombinase allows conditional genome editing in the mosquito  
965 stages of *Plasmodium berghei*. *PLoS One.* 2020;15.  
966 doi:10.1371/journal.pone.0236616
- 967 20. Mota MM, Pradel G, Vanderberg JP, Hafalla JC, Frevert U, Nussenzweig RS, et al.  
968 Migration of *Plasmodium* sporozoites through cells before infection. *Science.*  
969 2001;291: 141–144.
- 970 21. Richard D, MacRaild CA, Riglar DT, Chan JA, Foley M, Baum J, et al. Interaction  
971 between *Plasmodium falciparum* apical membrane antigen 1 and the rhoptry neck  
972 protein complex defines a key step in the erythrocyte invasion process of malaria  
973 parasites. *J Biol Chem.* 2010;285. doi:10.1074/jbc.M109.080770
- 974 22. Lamarque M, Besteiro S, Papoin J, Roques M, Vulliez-Le Normand B, Morlon-Guyot J,  
975 et al. The RON2-AMA1 interaction is a critical step in moving junction-dependent  
976 invasion by apicomplexan parasites. *PLoS Pathog.* 2011;7.  
977 doi:10.1371/journal.ppat.1001276
- 978 23. Srinivasan P, Beatty WL, Diouf A, Herrera R, Ambroggio X, Moch JK, et al. Binding of  
979 *Plasmodium* merozoite proteins RON2 and AMA1 triggers commitment to invasion.  
980 *Proc Natl Acad Sci U S A.* 2011;108. doi:10.1073/pnas.1110303108
- 981 24. Ecker A, Lewis RE, Eklund EH, Jayabalasingham B, Fidock DA. Tricks in  
982 *Plasmodium*'s molecular repertoire - Escaping 3'UTR excision-based conditional

- 983 silencing of the chloroquine resistance transporter gene. *Int J Parasitol.* 2012;42.  
984 doi:10.1016/j.ijpara.2012.09.003
- 985 25. Pimenta PF, Touray M, Miller L. The Journey of Malaria Sporozoites in the Mosquito  
986 Salivary Gland. *J Eukaryot Microbiol.* 1994;41: 608–624. doi:10.1111/j.1550-  
987 7408.1994.tb01523.x
- 988 26. Meis JFGM, Wismans PGP, Jap PHK, Lensen AHW, Ponnudurai T. A scanning  
989 electron microscopic study of the sporogonic development of *Plasmodium falciparum*  
990 in *Anopheles stephensi*. *Acta Trop.* 1992;50: 227–236. doi:10.1016/0001-  
991 706X(92)90079-D
- 992 27. Risco-Castillo V, Topçu S, Marinach C, Manzoni G, Bigorgne AE, Briquet S, et al.  
993 Malaria sporozoites traverse host cells within transient vacuoles. *Cell Host Microbe.*  
994 2015;18: 593–603. doi:10.1016/j.chom.2015.10.006
- 995 28. Schrevel J, Asfaux-Foucher G, Hopkins JM, Robert V, Bourgouin C, Prensier G, et al.  
996 Vesicle trafficking during sporozoite development in *Plasmodium berghei*:  
997 Ultrastructural evidence for a novel trafficking mechanism. *Parasitology.* 2008;135.  
998 doi:10.1017/S0031182007003629
- 999 29. Kudryashev M, Lepper S, Stanway R, Bohn S, Baumeister W, Cyrklaff M, et al.  
1000 Positioning of large organelles by a membrane- associated cytoskeleton in  
1001 *Plasmodium sporozoites*. *Cell Microbiol.* 2010;12: 362–371. doi:10.1111/j.1462-  
1002 5822.2009.01399.x
- 1003 30. Sinden RE, Strong K. An ultrastructural study of the sporogonic development of  
1004 *plasmodium falciparum* in *anopheles gambiae*. *Trans R Soc Trop Med Hyg.* 1978;72:  
1005 477–491. doi:10.1016/0035-9203(78)90167-0
- 1006 31. Guérin A, Corrales RM, Parker ML, Lamarque MH, Jacot D, El Hajj H, et al. Efficient  
1007 invasion by *Toxoplasma* depends on the subversion of host protein networks. *Nat*  
1008 *Microbiol.* 2017;2. doi:10.1038/s41564-017-0018-1
- 1009 32. Bichet M, Joly C, Hadj Henni A, Guilbert T, Xémard M, Tafani V, et al. The  
1010 *toxoplasma*-host cell junction is anchored to the cell cortex to sustain parasite invasive

- 1011 force. BMC Biol. 2014;12. doi:10.1186/s12915-014-0108-y
- 1012 33. Bichet M, Touquet B, Gonzalez V, Florent I, Meissner M, Tardieux I. Genetic  
1013 impairment of parasite myosin motors uncovers the contribution of host cell membrane  
1014 dynamics to Toxoplasma invasion forces. BMC Biol. 2016;14. doi:10.1186/s12915-  
1015 016-0316-8
- 1016 34. Collins CR, Hackett F, Howell SA, Snijders AP, Russell MR, Collinson LM, et al. The  
1017 malaria parasite sheddase sub2 governs host red blood cell membrane sealing at  
1018 invasion. Elife. 2020;9. doi:10.7554/ELIFE.61121
- 1019 35. Lamarque MH, Roques M, Kong-Hap M, Tonkin ML, Rugarabamu G, Marq J-B, et al.  
1020 Plasticity and redundancy among AMA-RON pairs ensure host cell entry of  
1021 Toxoplasma parasites. Nat Commun. 2014;5: 4098. doi:10.1038/ncomms5098
- 1022 36. Kappe SHI, Noe AR, Fraser TS, Blair PL, Adams JH. A family of chimeric erythrocyte  
1023 binding proteins of malaria parasites. Proc Natl Acad Sci U S A. 1998;95.  
1024 doi:10.1073/pnas.95.3.1230
- 1025 37. Kariu T, Yuda M, Yano K, Chinzei Y. MAEBL is essential for malarial sporozoite  
1026 infection of the mosquito salivary gland. J Exp Med. 2002;195: 1317–1323.  
1027 doi:10.1084/jem.20011876
- 1028 38. Saenz FE, Balu B, Smith J, Mendonca SR, Adams JH. The transmembrane isoform of  
1029 Plasmodium falciparum MAEBL is essential for the invasion of Anopheles salivary  
1030 glands. PLoS One. 2008;3: e2287. doi:10.1371/journal.pone.0002287
- 1031 39. Posthuma G, Meis JFGM, Verhave JP, Gigengack S, Hollingdale MR, Ponnudurai T,  
1032 et al. Immunogold determination of Plasmodium falciparum circumsporozoite protein in  
1033 Anopheles stephensi salivary gland cells. Eur J Cell Biol. 1989;49.
- 1034 40. Wells MB, Andrew DJ. Anopheles salivary gland architecture shapes plasmodium  
1035 sporozoite availability for transmission. MBio. 2019;10. doi:10.1128/mBio.01238-19
- 1036 41. Formaglio P, Tavares J, Ménard R, Amino R. Loss of host cell plasma membrane  
1037 integrity following cell traversal by Plasmodium sporozoites in the skin. Parasitol Int.  
1038 2014;63: 237–244. doi:10.1016/j.parint.2013.07.009



- 1039 42. Srinivasan P, Ekanem E, Diouf A, Tonkin ML, Miura K, Boulanger MJ, et al.  
1040 Immunization with a functional protein complex required for erythrocyte invasion  
1041 protects against lethal malaria. *Proc Natl Acad Sci U S A.* 2014;111.  
1042 doi:10.1073/pnas.1409928111
- 1043 43. Srinivasan P, Baldeviano GC, Miura K, Diouf A, Ventocilla JA, Leiva KP, et al. A  
1044 malaria vaccine protects Aotus monkeys against virulent *Plasmodium falciparum*  
1045 infection. *npj Vaccines.* 2017;2. doi:10.1038/s41541-017-0015-7
- 1046 44. Manzoni G, Briquet S, Risco-Castillo V. A rapid and robust selection procedure for  
1047 generating drug-selectable marker-free recombinant malaria parasites. *Sci Rep.*  
1048 2014;99210: 1–10. doi:10.1038/srep04760
- 1049 45. Ramakrishnan C, Delves MJ, Lal K, Blagborough AM, Butcher G, Baker KW, et al.  
1050 Laboratory maintenance of rodent malaria parasites. *Methods Mol Biol.* 2013;923: 51–  
1051 72. doi:10.1007/978-1-62703-026-7\_5
- 1052 46. Silvie O, Franetich JF, Boucheix C, Rubinstein E, Mazier D. Alternative invasion  
1053 pathways for *plasmodium berghei* sporozoites. *Int J Parasitol.* 2007;37: 173–182.  
1054 doi:10.1016/j.ijpara.2006.10.005
- 1055 47. Janse CJ, Ramesar J, Waters AP. High-efficiency transfection and drug selection of  
1056 genetically transformed blood stages of the rodent malaria parasite *Plasmodium*  
1057 *berghei*. *Nat Protoc.* 2006;1: 346–356. doi:10.1038/nprot.2006.53
- 1058 48. Perez-Riverol Y, Bai J, Bandla C, García-Seisdedos D, Hewapathirana S,  
1059 Kamatchinathan S, et al. The PRIDE database resources in 2022: A hub for mass  
1060 spectrometry-based proteomics evidences. *Nucleic Acids Res.* 2022;50.  
1061 doi:10.1093/nar/gkab1038
- 1062 49. Deerinck TJ, Bushong E a., Thor A, Ellisman MH. NCMIR methods for 3D EM: A new  
1063 protocol for preparation of biological specimens for serial block face scanning electron  
1064 microscopy. *Microscopy.* 2010; 6–8. Available:  
1065 [http://scholar.google.com/scholar?start=320&q=Mark+Ellisman&hl=en&as\\_sdt=0,5#0](http://scholar.google.com/scholar?start=320&q=Mark+Ellisman&hl=en&as_sdt=0,5#0)
- 1066 50. Walton J. Lead aspartate, an en bloc contrast stain particularly useful for

1067 ultrastructural enzymology. J Histochem Cytochem. 1979;27.

1068 doi:10.1177/27.10.512319

1069

1070

1071 **Supporting information**

1072 **Supplemental tables**

1073

1074 **S1 Table.** Mass spectrometry analysis of co-IP from RON4-mCherry sporozoites.

1075 **S2 Table.** List of oligonucleotides used in the study.

1076 **S3 Table.** Quantitative data and statistical analysis.

1077

1078

1079 **Supplemental figures**

1080

1081 **S1 Fig. Generation of *ama1*Δutr parasites using the DiCre system**

1082 **A.** Strategy to generate *ama1*Δutr parasites. The wild-type locus of *P. berghei ama1* in the  
1083 PbDiCre parasite line was targeted with a *ama1*Δutr replacement plasmid containing 2 Lox  
1084 sites and 5' and 3' homologous sequences inserted on each side of a GFP-2A-hDHFR  
1085 cassette. Upon double crossover recombination, the LoxN sites are inserted upstream of the  
1086 3' UTR and downstream of the GFP-2A-hDHFR cassette, respectively. Activation of the DiCre  
1087 recombinase with rapamycin results in excision of the 3' UTR together with the GFP-2A-  
1088 hDHFR cassette. Genotyping primers and expected PCR fragments are indicated by arrows  
1089 and lines, respectively. **B.** Genotyping of parental PbDiCre and *ama1*Δutr transfected parasites  
1090 after pyrimethamine selection (pyr) and after rapamycin treatment (rapa) of the final population.  
1091 Parasite genomic DNA was analyzed by PCR using primer combinations specific for the  
1092 unmodified locus (WT), the 5' integration, 3' integration or excision events. **C.** Flow cytometry  
1093 analysis of PbDiCre (parental) and *ama1*Δutr blood stage parasites after pyrimethamine  
1094 selection (pyr) or rapamycin exposure (rapa). NI, non-infected red blood cells.

1095

1096 **S2 Fig. Generation of *ama1*Con parasites using the DiCre system**

1097 **A.** Strategy to generate *ama1*Con parasites. The construct is similar to the *ama1*Δutr construct,  
1098 except that the first LoxN site is located downstream of the 3' UTR. Upon rapamycin-induced  
1099 excision, the *ama1* locus remains intact. **B.** Genotyping of parental PbDiCre and *ama1*Con  
1100 transfected parasites after pyrimethamine selection (pyr) and after rapamycin treatment (rapa)  
1101 of the final population. Parasite genomic DNA was analyzed by PCR using primer  
1102 combinations specific for the unmodified locus (WT), the 5' integration, 3' integration or  
1103 excision events. **C.** Flow cytometry analysis of PbDiCre (parental) and *ama1*Con blood stage  
1104 parasites after pyrimethamine selection (pyr) or rapamycin exposure (rapa). NI, non-infected  
1105 red blood cells.

1106

1107 **S3 Fig. Imaging of *ama1*Con and *ama1*Δutr mosquito stages**

1108 **A.** Fluorescence microscopy images of midguts from mosquitoes infected with untreated (UT)  
1109 or rapamycin-treated (rapa) *ama1*Con and *ama1*Δutr parasites. Scale bar = 200 μm. **B.**  
1110 Fluorescence microscopy images of salivary glands from mosquitoes infected with untreated  
1111 (UT) or rapamycin-treated (rapa) *ama1*Con and *ama1*Δutr parasites. Scale bar = 200 μm.

1112

1113 **S4 Fig. Generation of *ama1*cKO parasites using the DiCre system**

1114 **A.** Strategy to generate *ama1*cKO parasites. The *ama1* locus in rapamycin-treated (excised)  
1115 *ama1*Con parasites was targeted with a *ama1*cKO replacement plasmid containing a single  
1116 LoxN site and 5' and 3' homologous sequences inserted on each side of a GFP-2A-hDHFR  
1117 cassette. Upon double crossover recombination, a second LoxN site is inserted upstream of  
1118 the GFP-2A-hDHFR cassette and *ama1* gene. Activation of the DiCre recombinase with  
1119 rapamycin results in excision of the entire *ama1* gene together with the GFP-2A-hDHFR  
1120 cassette. Genotyping primers and expected PCR fragments are indicated by arrows and lines,  
1121 respectively. **B.** Genotyping of PbDiCre, rapamycin-treated (excised) *ama1*Con (parental) and  
1122 *ama1*cKO parasites after selection with pyrimethamine (pyr). Parasite genomic DNA was  
1123 analyzed by PCR using primer combinations specific for the unmodified locus (WT), the 5'  
1124 integration and 3' integration events. **C.** Genotyping of *ama1*cKO blood stage parasites

1125 collected 2 or 6 days after rapamycin exposure or left untreated (UT). Parasite genomic DNA  
1126 was analyzed by PCR using primer combinations specific for the non-excised (NE, 5'  
1127 integration combination) or excised (E) locus.

1128

### 1129 **S5 Fig. Imaging of *ama1*cKO mosquito stages**

1130 **A.** Fluorescence microscopy of midguts from mosquitoes infected with untreated (UT) or  
1131 rapamycin-treated (rapa) *ama1*cKO parasites. Scale bar = 200  $\mu$ m. **B.** Fluorescence  
1132 microscopy of salivary glands isolated from mosquitoes infected with untreated (UT) or  
1133 rapamycin-treated (rapa) *ama1*cKO parasites. Scale bar = 200  $\mu$ m.

1134

### 1135 **S6 Fig. Analysis of mosquito pericardial structures**

1136 **A.** Imaging of the abdomen of a mosquito infected with rapamycin treated *ama1*cKO parasites,  
1137 after removal of the midgut, showing mCherry-labelled pericardial structures. **B.** Quantification  
1138 of mosquitoes with mCherry-labelled pericardial cells at D21 post-infection with untreated (UT)  
1139 or rapamycin-treated (rapa) *ama1*Con and *ama1*cKO parasites. Ns, non-significant (Two-tailed  
1140 ratio paired t test).

1141

### 1142 **S7 Fig. Generation of *ron2*cKO parasites using the DiCre system**

1143 **A-B.** Two-step strategy to generate *ron2*cKO parasites. In the first step (**A**), the *ron2* locus in  
1144 PbDiCre parasites was targeted with a *ron2*-P1 replacement plasmid containing 5' and 3'  
1145 homologous sequences and two LoxN sites flanking a GFP-2A- hDHFR cassette. Upon double  
1146 crossover recombination, the two LoxN sites are inserted upstream of *ron2*. Activation of the  
1147 DiCre recombinase with rapamycin results in excision of the GFP-2A-hDHFR cassette, leaving  
1148 a single LoxN site upstream of the gene in excised *ron2*-P1 parasites. In the second step (**B**),  
1149 the *ron2* locus in rapamycin-treated (excised) *ron2*-P1 parasites was targeted with a *ron2*-P2  
1150 replacement plasmid containing 5' and 3' homologous sequences flanking a GFP-2A- hDHFR  
1151 cassette and a single LoxN site. Upon double crossover recombination, the LoxN site is  
1152 inserted downstream of *ron2* and the GFP-2A- hDHFR cassette. Activation of the DiCre  
1153 recombinase with rapamycin results in excision of the entire *ron2* gene together with the GFP-  
1154 2A-hDHFR cassette. Genotyping primers and expected PCR fragments are indicated by  
1155 arrows and lines, respectively. **C.** Genotyping of PbDiCre and *ron2*cKO parasites. Parasite  
1156 genomic DNA was analyzed by PCR using primer combinations specific for the unmodified  
1157 locus (WT), the 5' and 3' integration events.

1158

### 1159 **S8 Fig. Generation of *ron4*cKO parasites using the DiCre system**

1160 **A-B.** Two-step strategy to generate *ron4*cKO parasites. In the first step (**A**), the *ron4* locus in  
1161 PbDiCre parasites was targeted with a *ron2*-P1 replacement plasmid containing 5' and 3'  
1162 homologous sequences and two LoxN sites flanking a GFP-2A- hDHFR cassette. Upon double  
1163 crossover recombination, the two LoxN sites are inserted upstream of *ron4*. Activation of the  
1164 DiCre recombinase with rapamycin results in excision of the GFP-2A-hDHFR cassette, leaving  
1165 a single LoxN site upstream of the gene in excised *ron4*-P1 parasites. In the second step (**B**),  
1166 the *ron4* locus in rapamycin-treated (excised) *ron4*-P1 parasites was targeted with a *ron4*-P2  
1167 replacement plasmid containing 5' and 3' homologous sequences flanking a GFP-2A- hDHFR  
1168 cassette and a single LoxN site. Upon double crossover recombination, the LoxN site is  
1169 inserted downstream of *ron4* and the GFP-2A- hDHFR cassette. Activation of the DiCre  
1170 recombinase with rapamycin results in excision of the entire *ron4* gene together with the GFP-  
1171 2A-hDHFR cassette. Genotyping primers and expected PCR fragments are indicated by  
1172 arrows and lines, respectively. **C.** Genotyping of PbDiCre and *ron4*cKO parasites. Parasite  
1173 genomic DNA was analyzed by PCR using primer combinations specific for the unmodified  
1174 locus (WT), the 5' and 3' integration events.

1175

### 1176 **S9 Fig. Imaging of *ron2*cKO and *ron4*cKO mosquito stages**

1177 **A-B.** Fluorescence microscopy of midguts from mosquitoes infected with untreated (UT) or  
1178 rapamycin-treated (rapa) *ron2*cKO (**A**) or *ron4*cKO (**B**) parasites. Scale bar = 200  $\mu$ m.

1179

### 1180 **S10 Fig. Analysis of mosquito pericardial structures**

1181 Quantification of mosquitoes with mCherry-labelled pericardial cells at D21 post-infection with  
1182 untreated (UT) or rapamycin-treated (rapa) *ron2cKO* or *ron4cKO* parasites. Ns, non-significant  
1183 (Two-tailed ratio paired t test).

1184  
1185 **S11 Fig. Serial block face-scanning electron microscopy (SBF-SEM) of infected**  
1186 **mosquito salivary glands**

1187 **A-B.** Representative sections of salivary glands from mosquitoes infected with WT (**A**) or  
1188 rapamycin-treated *ama1cKO* (**B**) parasites (left panels). Scale bars, 5  $\mu\text{m}$ . WT and AMA1-  
1189 deficient sporozoites were observed inside the acinar cells (AC, asterisks) and in the secretory  
1190 cavities (SC, arrows). The volume segmentation images (right panels) show the secretory  
1191 cavities (yellow) and sporozoites (blue), and correspond to Movie 1 and Movie 2, respectively,  
1192 for WT and *ama1cKO* parasites.

1193  
1194 **S12 Fig. SBF-SEM analysis of sporozoite distribution inside salivary glands**

1195 **A-B.** SBF-SEM sections from Movie 3, showing WT sporozoites inside salivary gland acinar  
1196 cells. The first section (**A**) shows a sporozoite partly surrounded by host cell membranes  
1197 (arrow), highlighted in red in the right panel, and a second one seemingly contained inside a  
1198 vacuole (asterisk), highlighted in yellow in the right panel. The second section (**B**) shows the  
1199 same parasites in a different plane, revealing that the second sporozoite is in fact not enclosed  
1200 in a vacuole but instead is interacting with invaginated host cell membranes (asterisk),  
1201 highlighted in yellow in the right panel, while the first parasite now seems surrounded by a  
1202 membrane (arrow), giving the false impression of being enclosed in a vacuole (highlighted in  
1203 red in the right panel). Scale bars, 2  $\mu\text{m}$ . **C.** SBF-SEM section showing an intracellular  
1204 rapamycin-treated *ama1cKO* sporozoite surrounded by a cellular membrane (arrow). Scale  
1205 bar, 2  $\mu\text{m}$ . AC, acinar cell; SC, secretory cavity. **D-E.** SBF-SEM sections showing WT (**D**) and  
1206 rapamycin-treated *ama1cKO* (**E**) sporozoites present inside secretory cavities (SC) and  
1207 surrounded by cellular membranes (arrows). Scale bars, 1  $\mu\text{m}$ .

1208  
1209 **S13 Fig. SBF-SEM imaging of sporozoite invasion into mosquito salivary glands**

1210 **A-H.** SBF-SEM images of an invading untreated *ama1cKO* sporozoite. Panels A-C show three  
1211 XY sections of the invading parasite. The sporozoite is located underneath the basal lamina  
1212 (BL), and enters the cell surrounded by a vacuole (white arrowhead). The entry site is marked  
1213 by a black arrow. Scale bar, 1  $\mu\text{m}$ . Panel D shows a virtual XZ section, illustrating that the  
1214 sporozoite is penetrating tangentially into the acinar cell. The entry aperture is marked by a  
1215 black arrowhead. Panels E-H show a volume segmentation of the parasite (in purple) invading  
1216 the mosquito cell (in yellow). The entry site is marked by a black arrowhead. In G and H, only  
1217 the cell surface is shown, revealing the imprinting of the extracellular portion of the sporozoite  
1218 (black arrow). In H, the circular entry site is shown at higher magnification. **I-K.** SBF-SEM  
1219 images of another invading untreated *ama1cKO* sporozoite. In I, a XY section cuts the invading  
1220 parasite twice (black arrows), with the extracellular portion being positioned between the cell  
1221 surface and the basal lamina (BL). Two virtual YZ sections are shown in J and K, illustrating  
1222 that the sporozoite is penetrating tangentially into the acinar cell. The entry aperture is marked  
1223 by a black arrowhead. A full rhoptry is visible in J and an empty one can be seen in K (arrows).

1224  
1225 **S14 Fig. SBF-SEM imaging of sporozoite rhoptries**

1226 **A-B.** SBF-SEM sections of the apical end of an intracellular untreated (wt) *ama1cKO*  
1227 sporozoite. In A, two full rhoptries are visible, indicated by white arrows. In B, a different section  
1228 of the same parasite reveals an empty rhoptry (black arrow). **C.** SBF-SEM section of an  
1229 intracellular rapamycin-treated *ron2cKO* sporozoite, showing two full rhoptries (white arrows)  
1230 and one empty one (black arrow). Scale bars, 1  $\mu\text{m}$ .

1231  
1232  
1233 **S15 Fig. SBF-SEM imaging of RON2-deficient sporozoite invasion into mosquito**  
1234 **salivary glands**

1235 **A-F.** SBF-SEM images of two invading rapamycin-treated *ron2cKO* sporozoites. In A, the first  
1236 sporozoite (labelled #1) is cut once, while the second one (#2) is cut twice. The entry sites are

1237 indicated by black arrows, and the vacuoles by white arrowheads. Scale bars, 1  $\mu\text{m}$ . Panels B  
1238 and C show volume segmentation images of the invading parasites (red and purple,  
1239 respectively). The cell is colored in yellow. Panel D shows a virtual XZ section, showing the  
1240 vacuole (white arrowhead), a full rhoptry (black arrow) and an empty vesicle (white arrow). **G-**  
1241 **J.** SBF-SEM images of another rapamycin-treated *ron2cKO* sporozoites. In G, the entry site is  
1242 indicated by a black arrow, and the vacuole by a white arrowhead. Panels H-J show volume  
1243 segmentation images of the invading parasite (purple). The cell is colored in yellow. The entry  
1244 site is shown at higher magnification in I and J, with or without displaying the sporozoite.  
1245

1246 **S16 Fig. SBF-SEM imaging of AMA1- and RON2-deficient sporozoites inside salivary**  
1247 **gland cells**

1248 **A-B.** SBF-SEM sections of intracellular rapamycin-treated *ama1cKO* (A) and *ron2cKO* (B)  
1249 sporozoites. Both parasites display a strong bending, with the hinge indicated by an arrow.  
1250 Scale bars, 2  $\mu\text{m}$ .  
1251

1252 **S17 Fig. Cellular alterations in heavily infected mosquito salivary glands**

1253 **A.** SBF-SEM section showing an alteration of the cellular interface with the secretory cavity at  
1254 the point of entry of multiple WT sporozoites (asterisk). Intraluminal leakage of cytoplasmic  
1255 material is indicated with an arrow. Scale bar, 5  $\mu\text{m}$ . **B.** Fluorescence microscopy images of  
1256 salivary gland distal lobes infected with rapamycin-treated *ama1Con* or untreated *ron2cKO*  
1257 parasites. Samples were stained with Phalloidin-iFluor 647 (magenta) and Hoechst 77742  
1258 (Blue). The right panels show mCherry (red), GFP (green) and Hoechst (blue) merge images.  
1259 In both cases, the heavy parasite load is associated with internal alterations of the phalloidin  
1260 staining, but the basal border of the lobes is preserved. Scale bars, 50  $\mu\text{m}$ .  
1261

1262 **S18 Fig. Infection by AMA1- and RON2-deficient parasites is associated with a loss of**  
1263 **integrity of the mosquito salivary gland epithelium**

1264 Representative fluorescence microscopy images of salivary gland lobes infected with  
1265 untreated (UT) or rapamycin-treated (+Rapa) *ama1cKO* or *ron2cKO* parasites, day 16 post-  
1266 infection. Samples were stained with Phalloidin-iFluor 647 (magenta) and Hoechst 77742  
1267 (Blue). The right panels show mCherry (red), GFP (green) and Hoechst (blue) merge images.  
1268 Zones of retraction of the acinar epithelial cells are visible in the lobes infected with AMA1-  
1269 and RON2-deficient sporozoites (arrows). Scale bars, 50  $\mu\text{m}$ .  
1270

1271  
1272 **Supplemental movies**

1273  
1274 **Movie 1.** 3D segmentation of a mosquito salivary gland infected with WT (PbGFP) sporozoites,  
1275 day 21 post-feeding. Parasites appear in blue and secretory cavities in yellow. This movie  
1276 corresponds to Fig S11A.  
1277

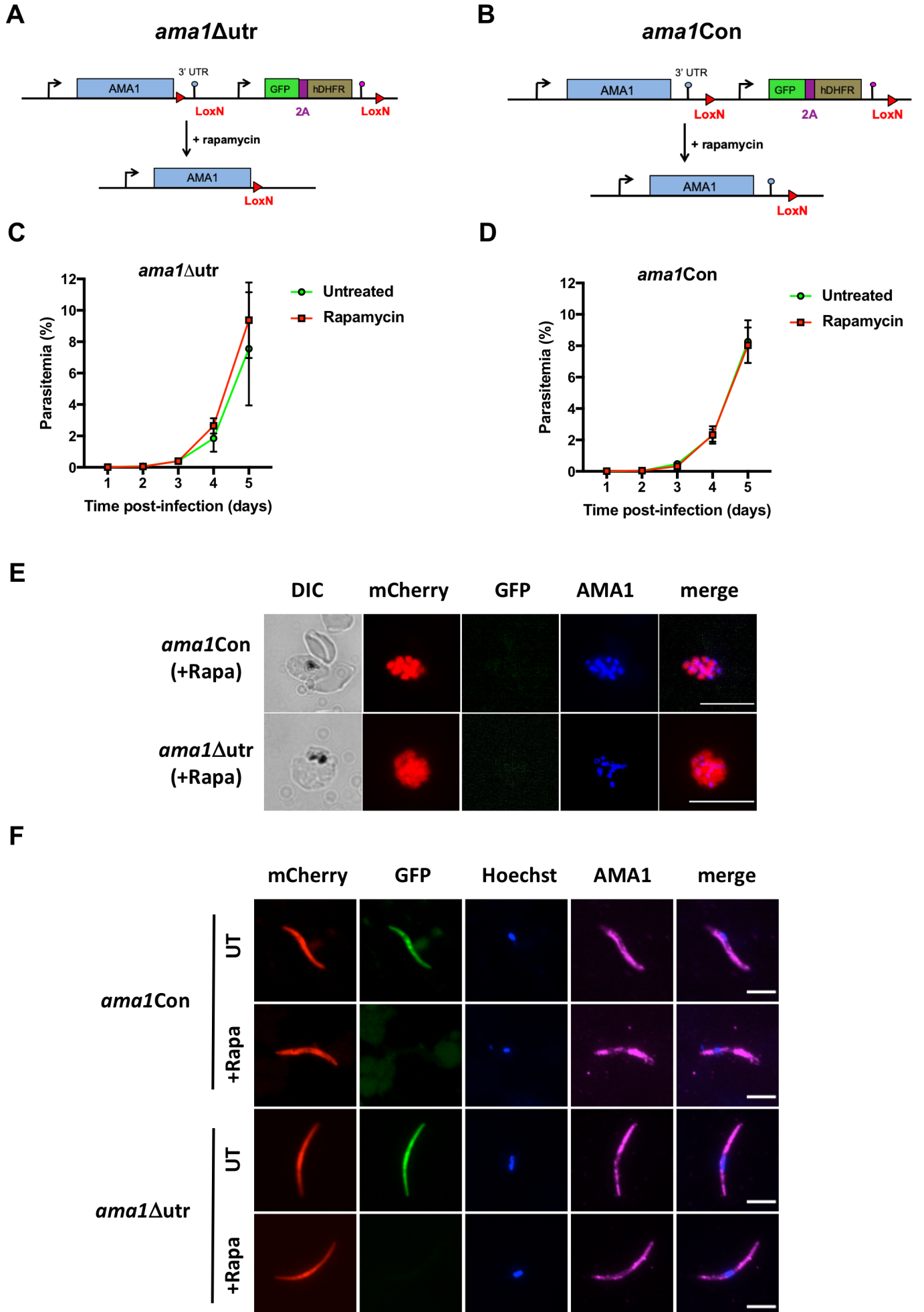
1278 **Movie 2.** 3D segmentation of a mosquito salivary gland infected with rapamycin-treated  
1279 *ama1cKO* sporozoites, day 21 post-feeding. Parasites appear in blue and secretory cavities in  
1280 yellow. This movie corresponds to Fig S11B.  
1281

1282 **Movie 3.** SBF-SEM sections of a mosquito salivary gland infected with WT parasites, day 21  
1283 post-feeding. This movie corresponds to Fig S12A-B.  
1284

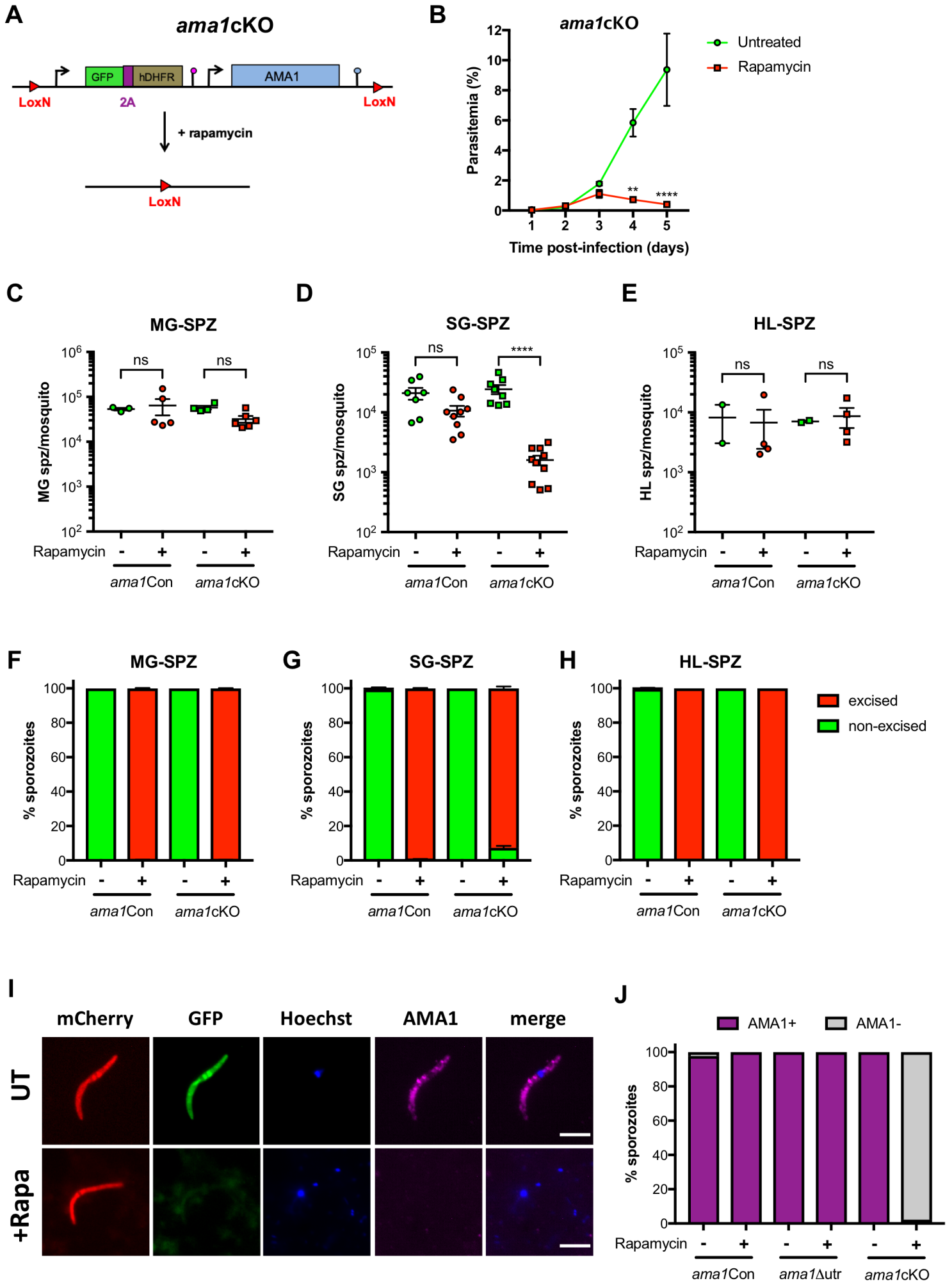
1285 **Movie 4.** 3D segmentation of an untreated *ama1cKO* sporozoite invading a salivary gland cell,  
1286 day 15 post-feeding. The invading parasite is colored in purple and the acinar cell in yellow.  
1287 This movie corresponds to Fig 5A-F.  
1288

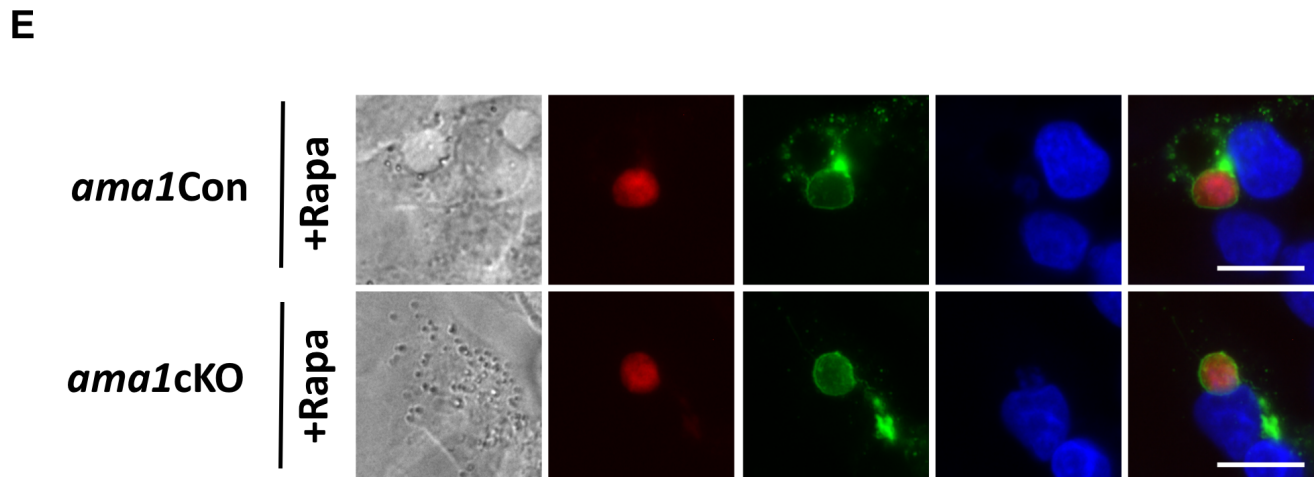
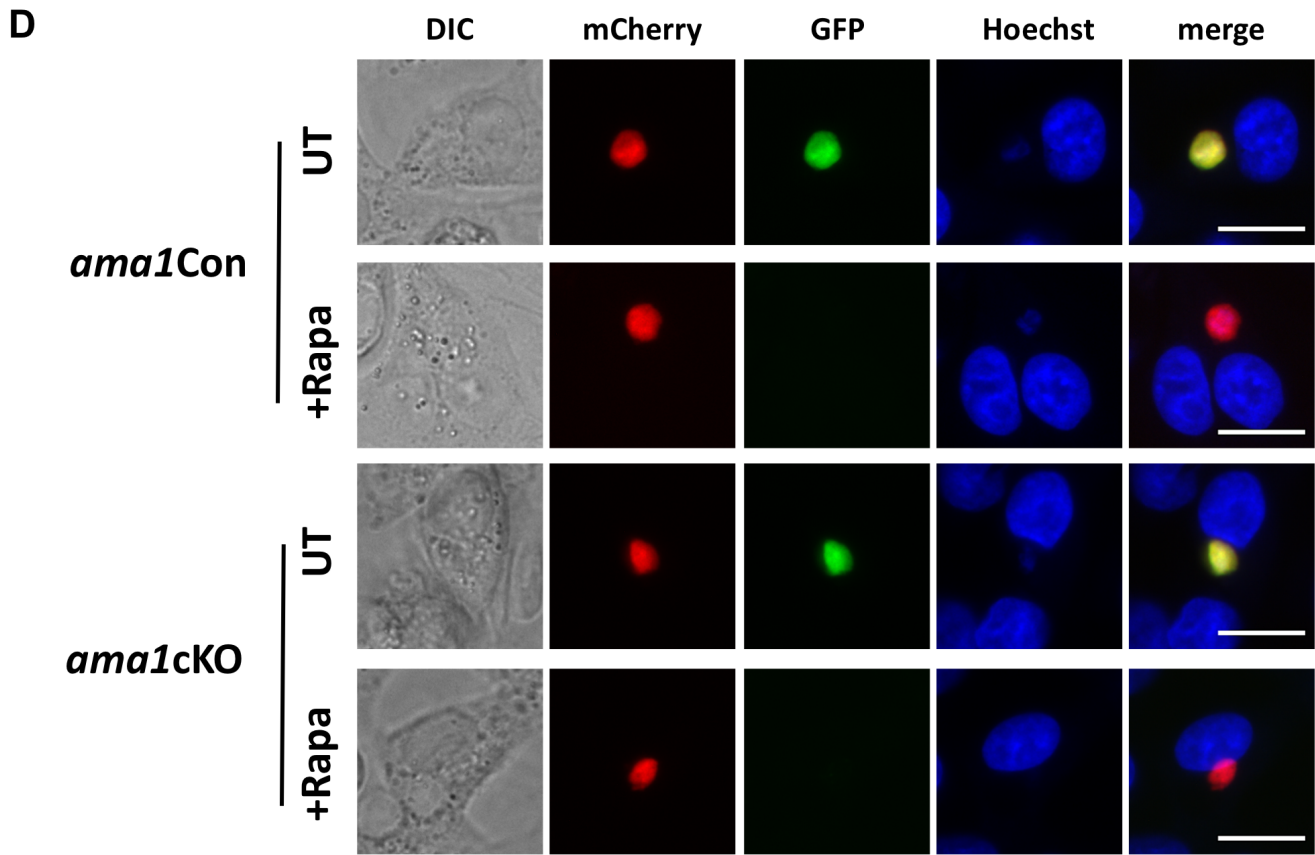
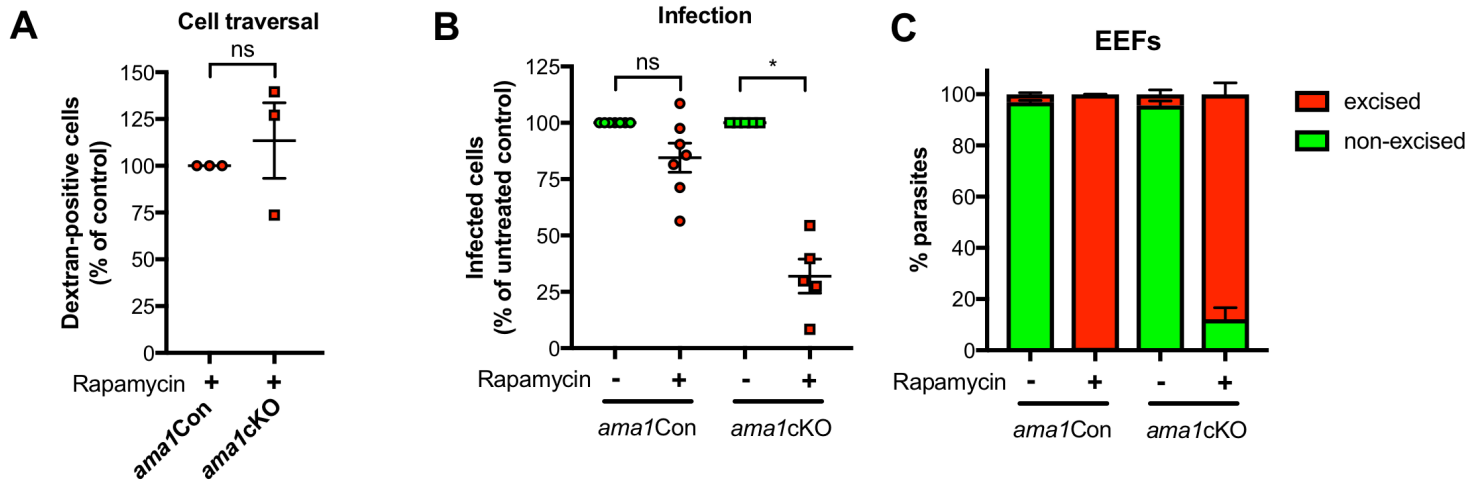
1289 **Movie 5.** 3D segmentation of the same invading untreated *ama1cKO* sporozoite as in Movie  
1290 4, highlighting the apical organelles. The parasite appears in pink, full rhoptries in blue and  
1291 empty vesicles in green. This movie corresponds to Fig 5A-C.  
1292

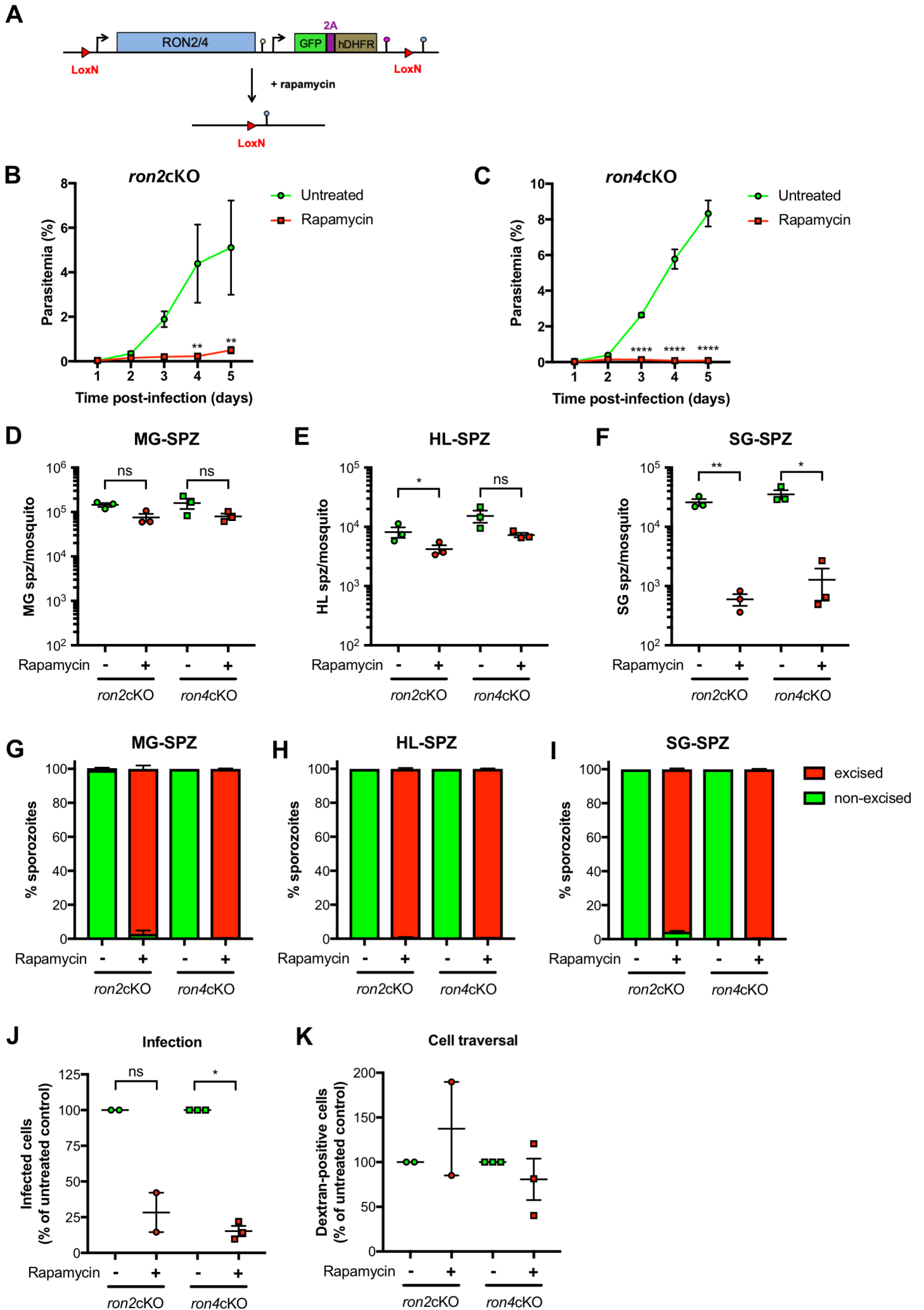
1293 **Movie 6.** 3D segmentation of a rapamycin-treated *ron2cKO* sporozoite invading a salivary  
1294 gland cell, day 15 post-feeding. The invading parasite is colored in purple and the acinar cell  
1295 in yellow. This movie corresponds to Fig 5G-K.  
1296

**Fig1**



**Fig2**

**Fig3**

**Fig4**

**Fig5**

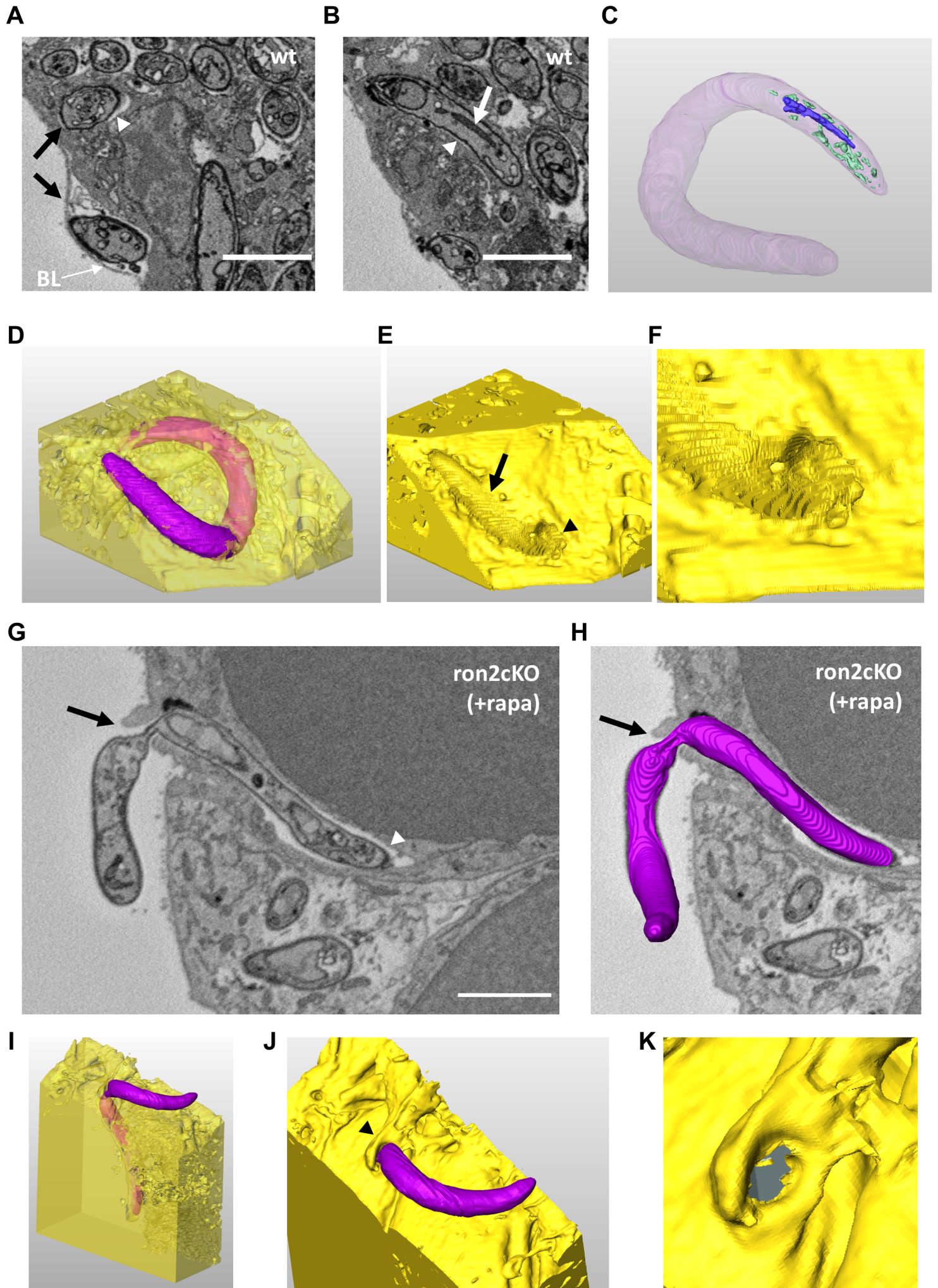


**Fig6**

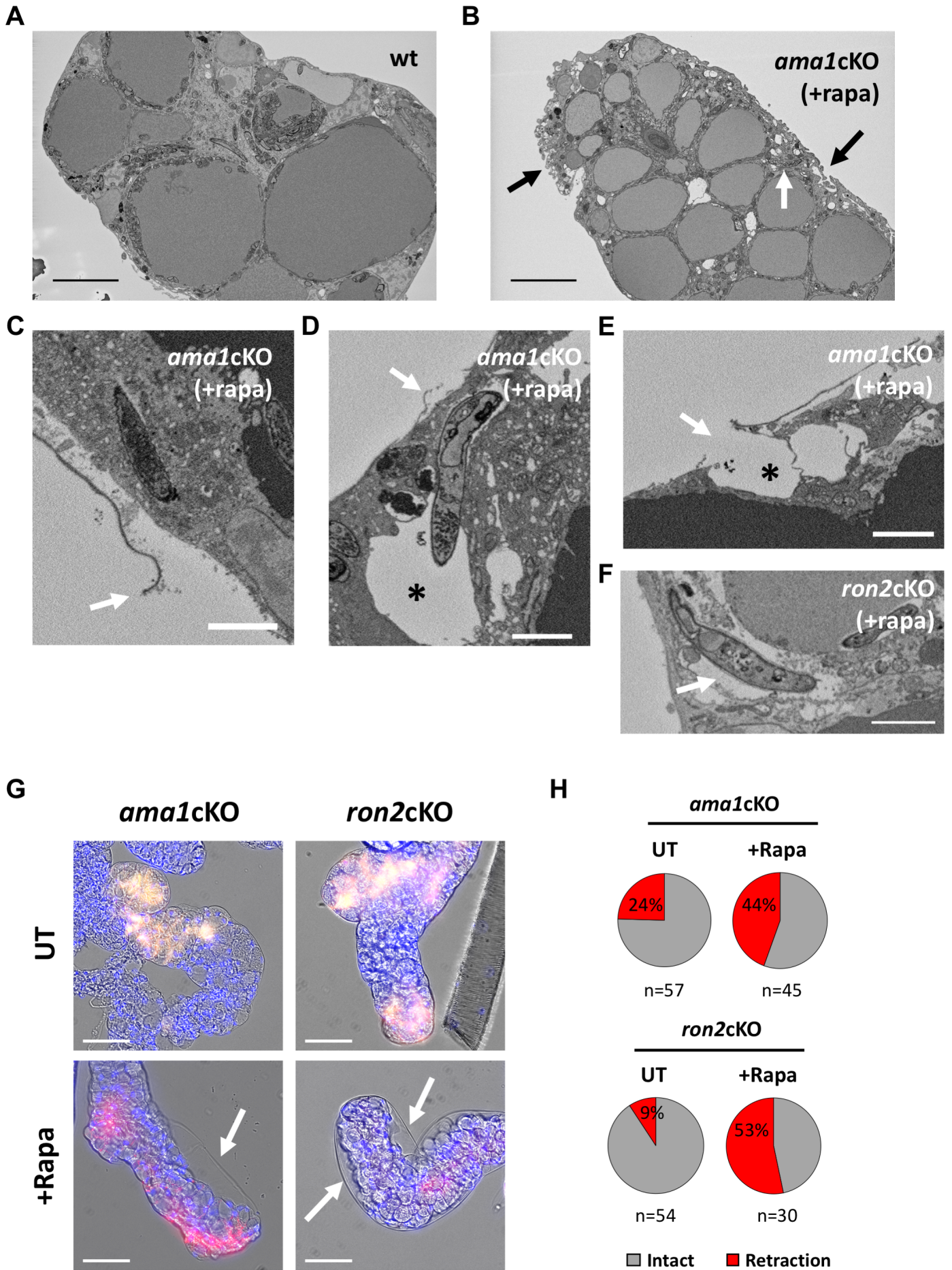
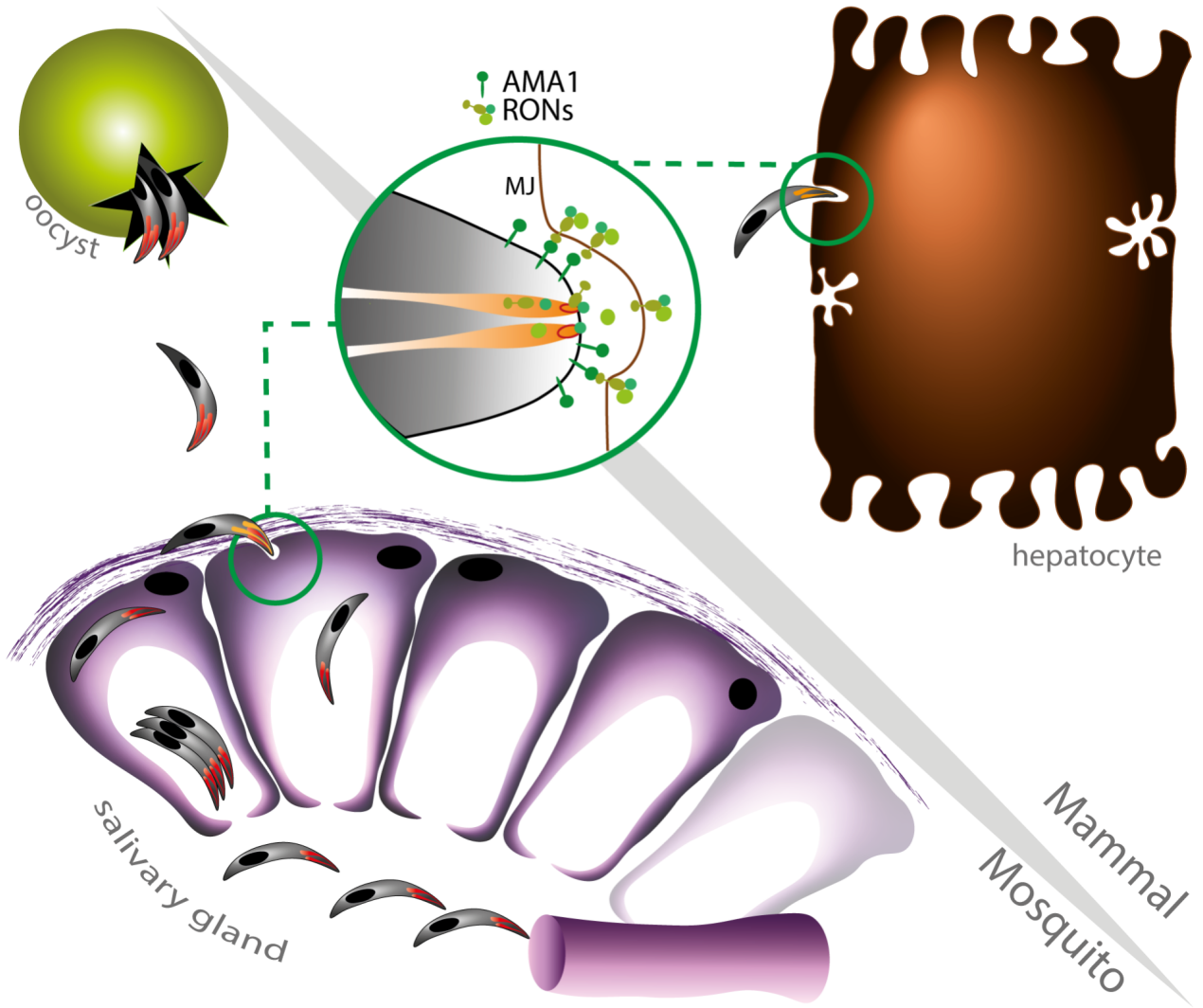
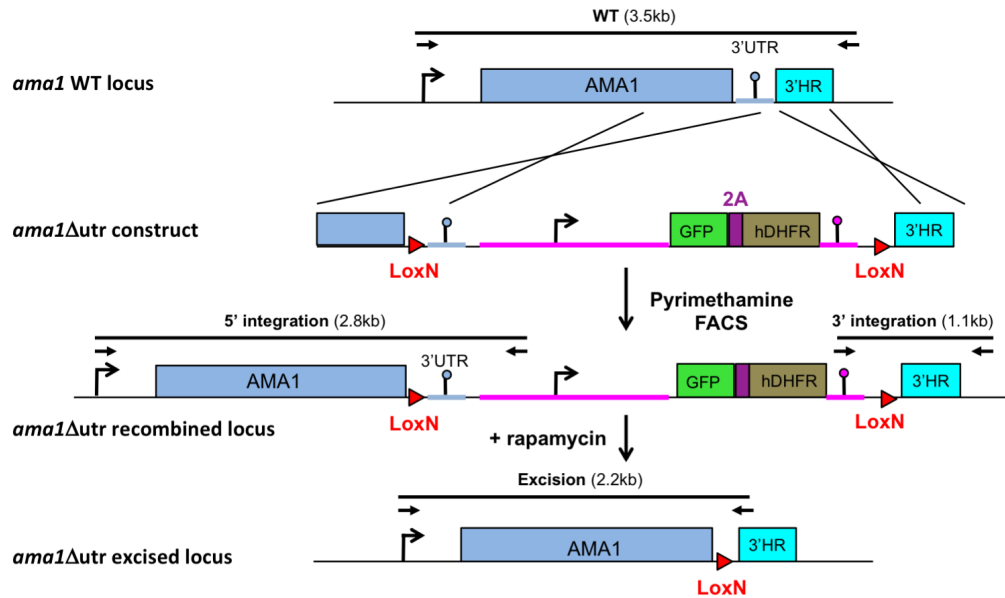


Fig7

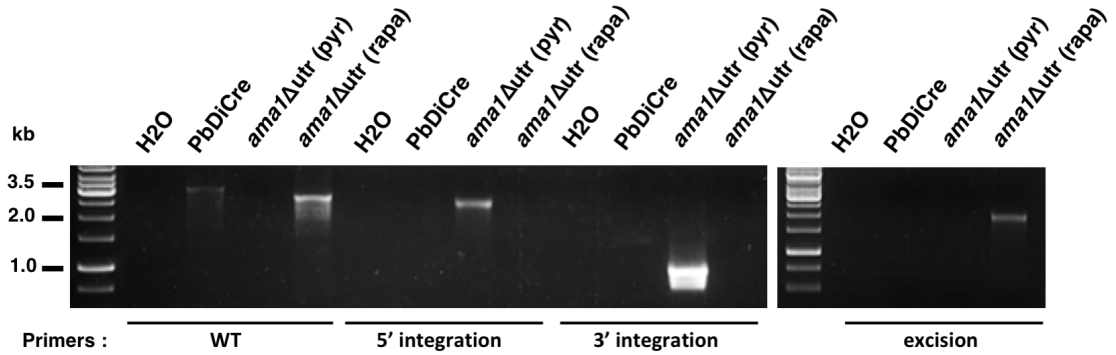


**FigS1**

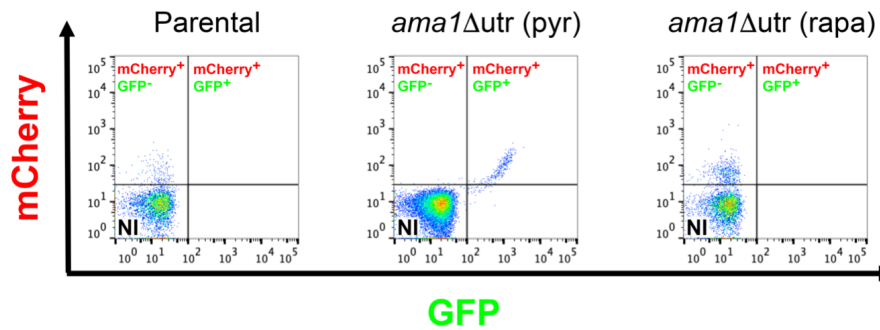
**A**



**B**

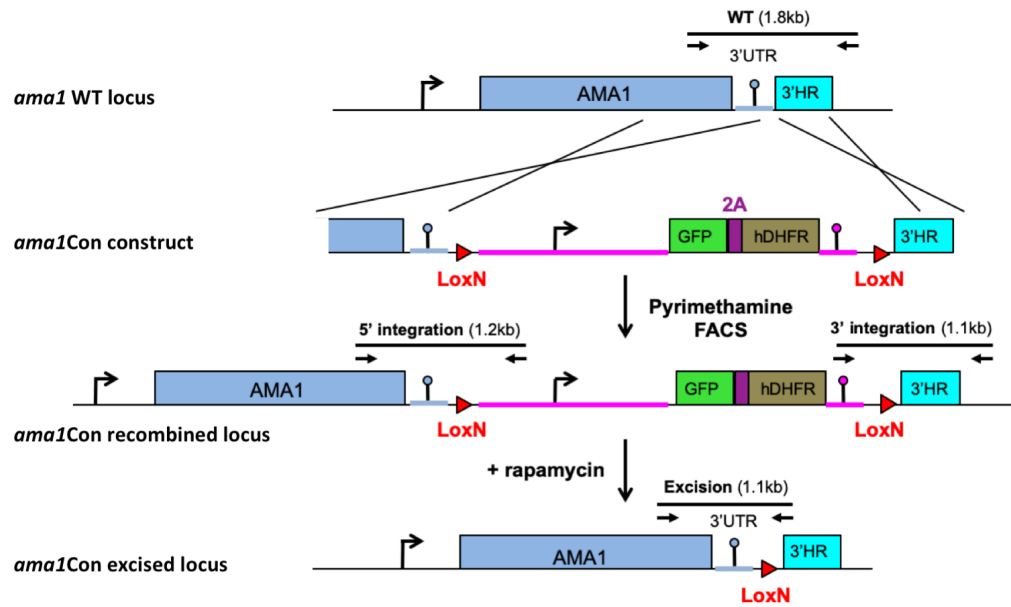


**C**

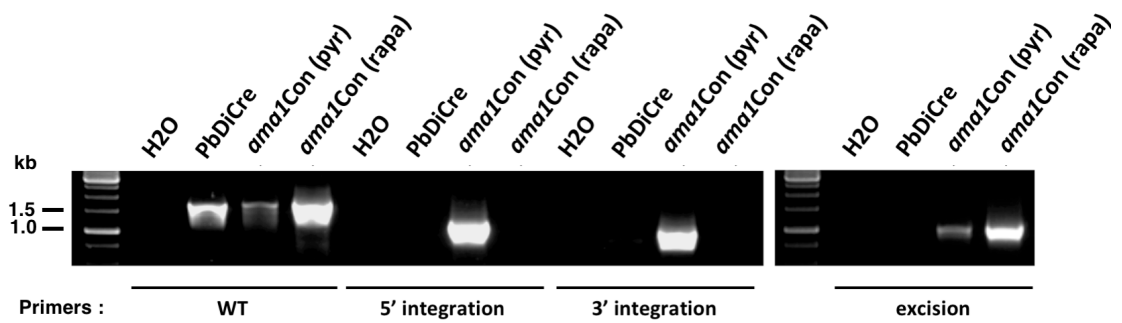


FigS2

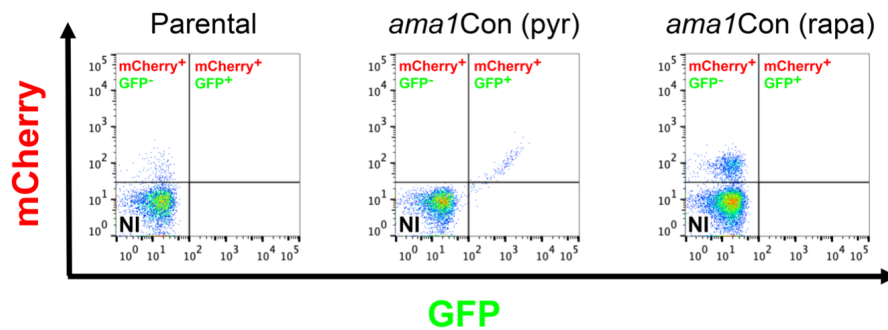
A



B



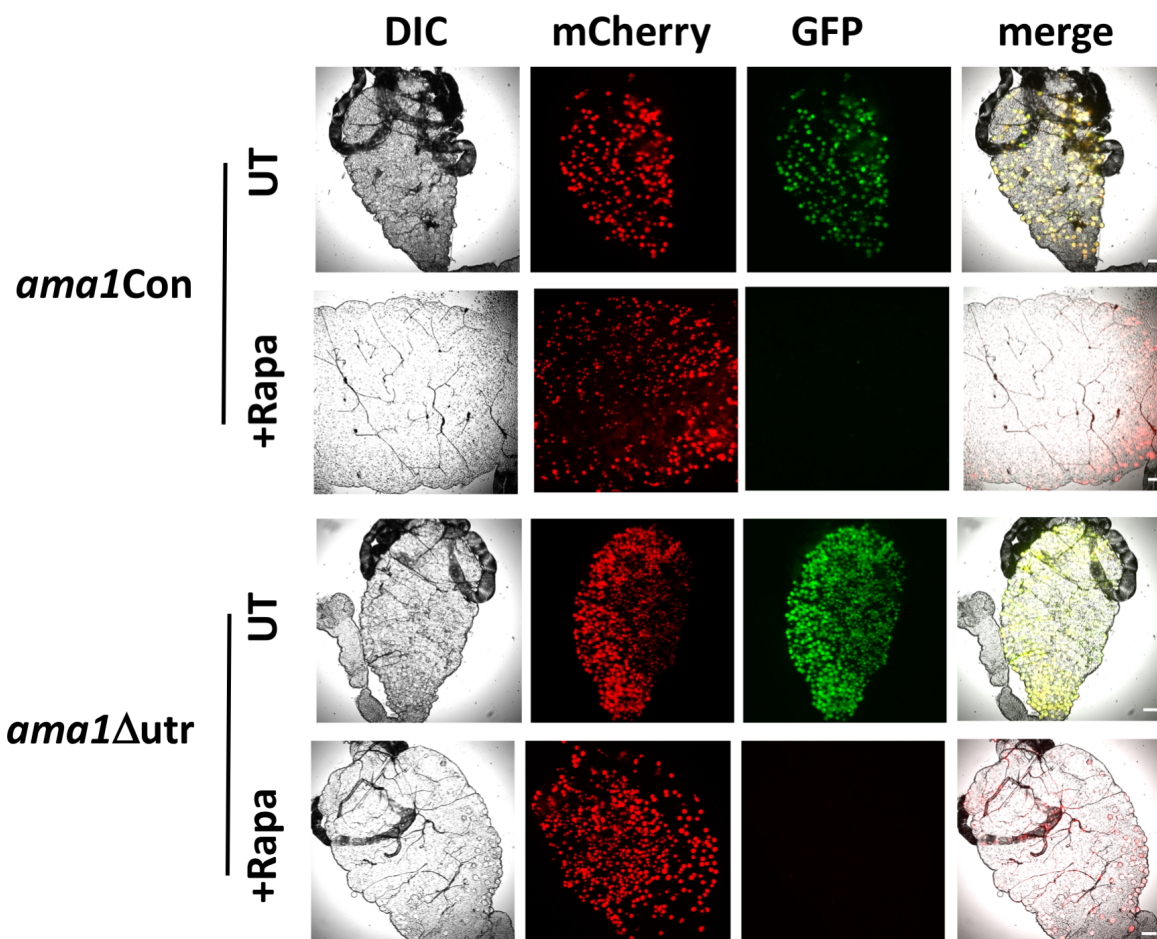
C



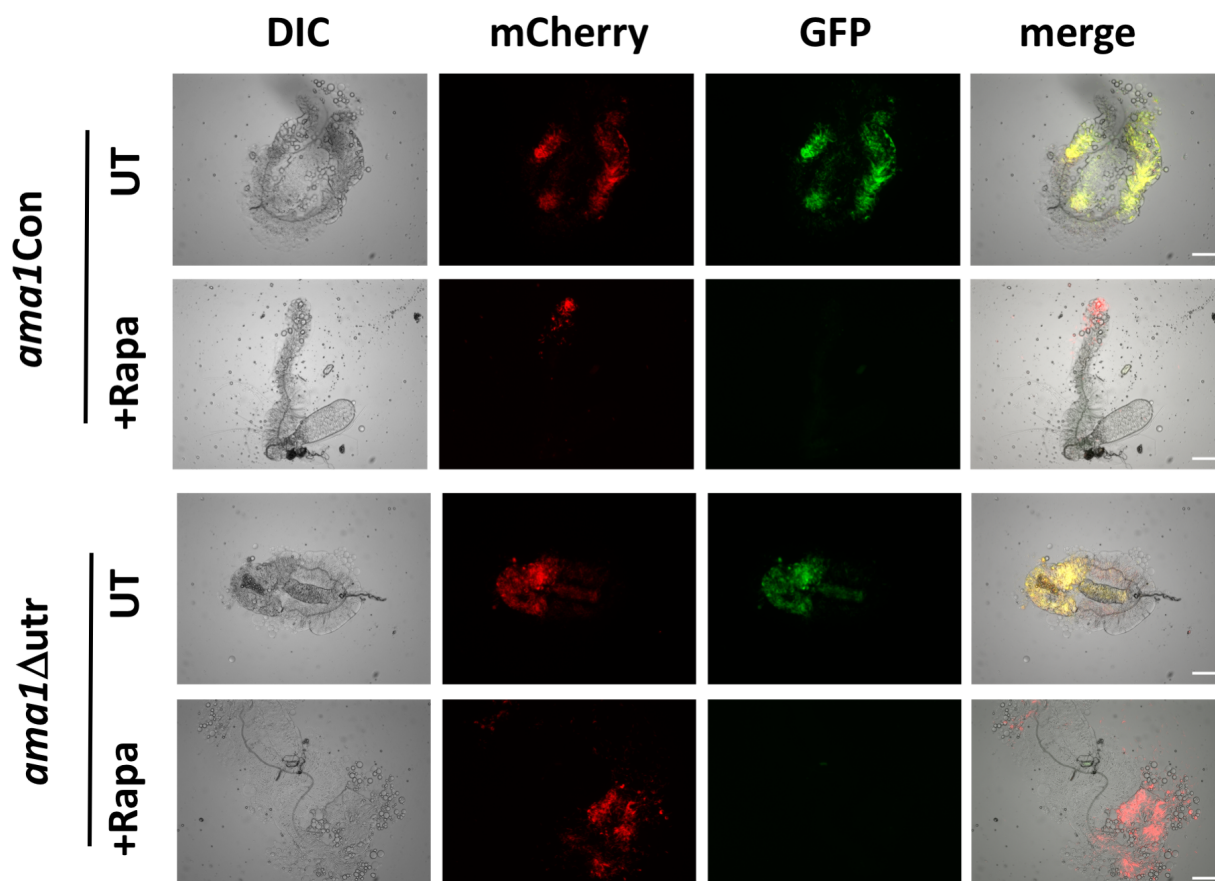


FigS3

A

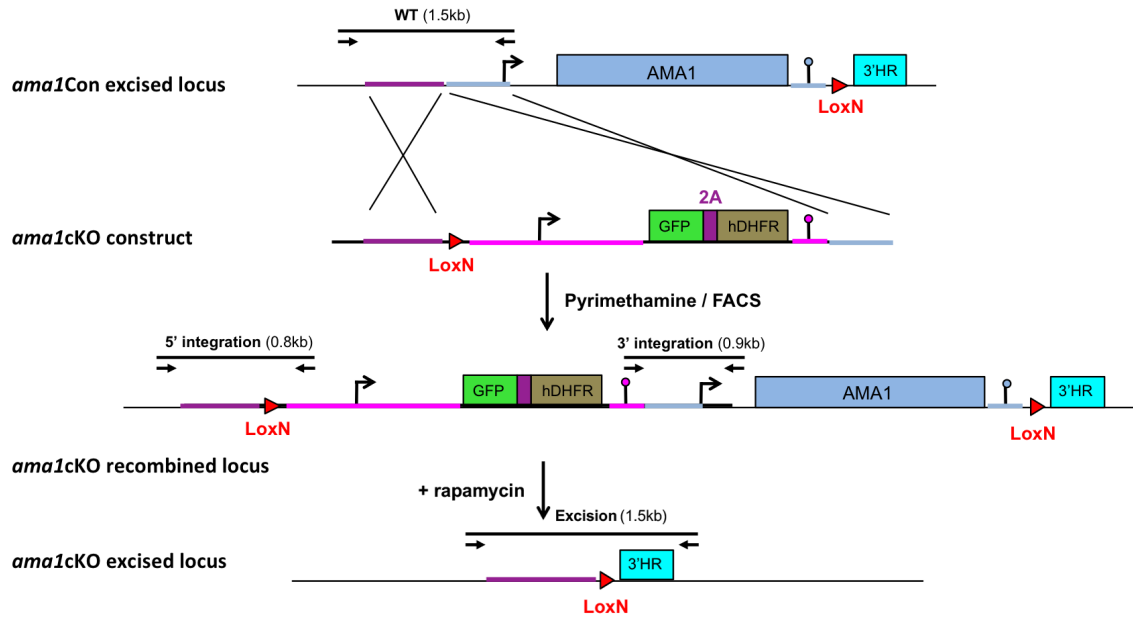


B

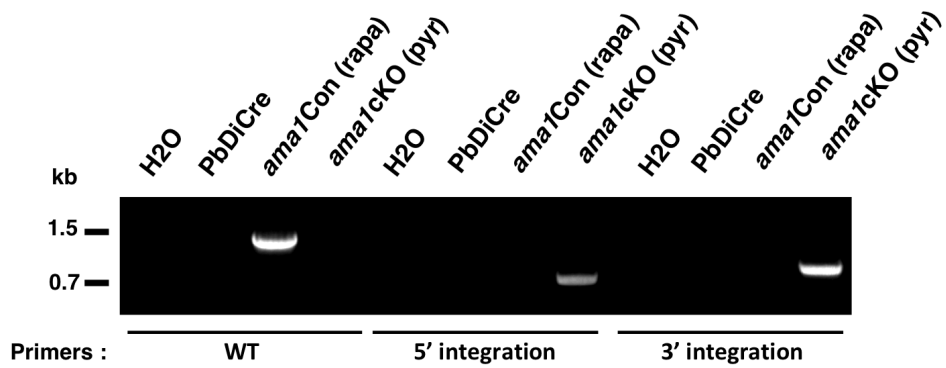


**FigS4**

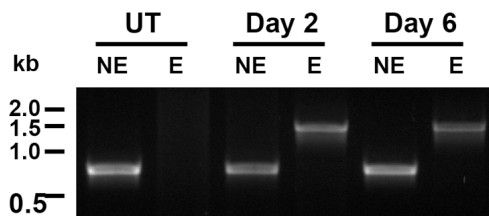
**A**



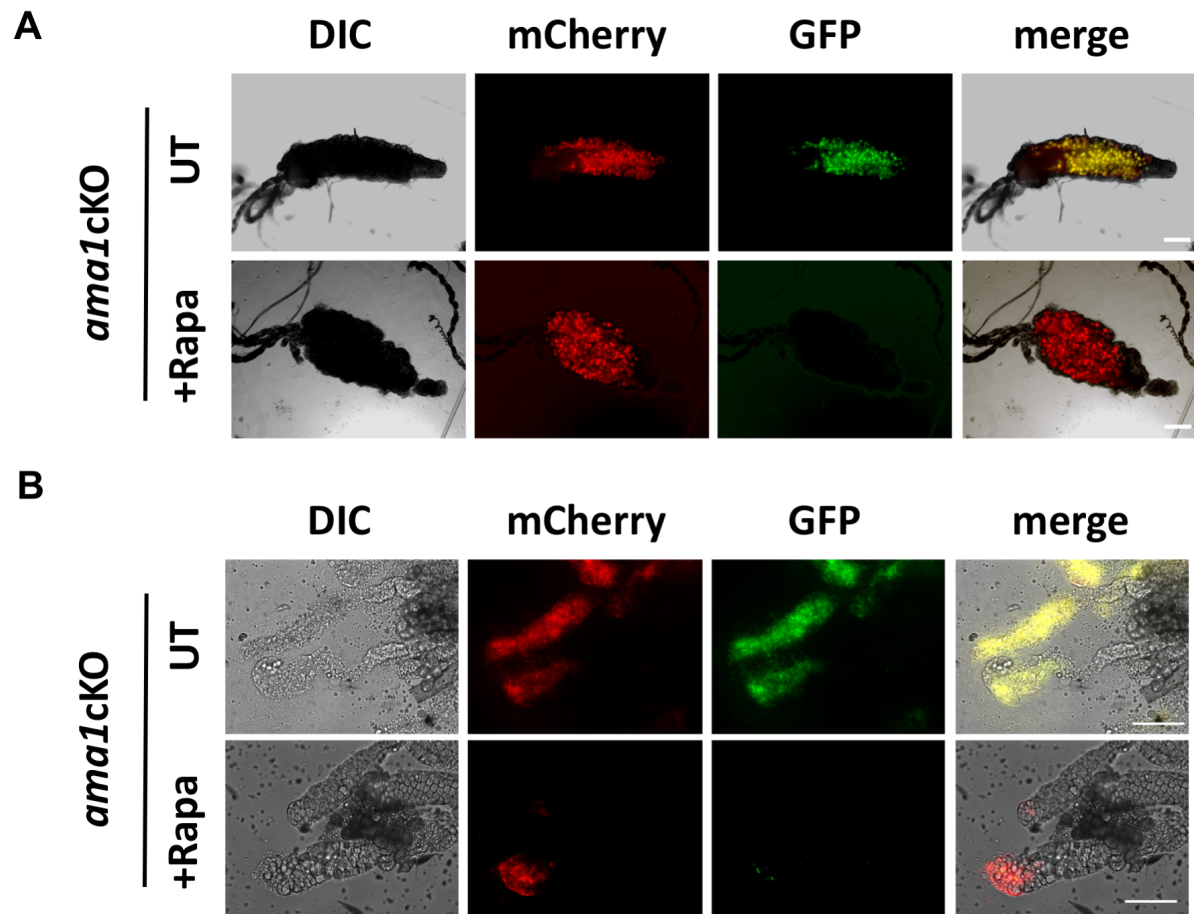
**B**



**C**

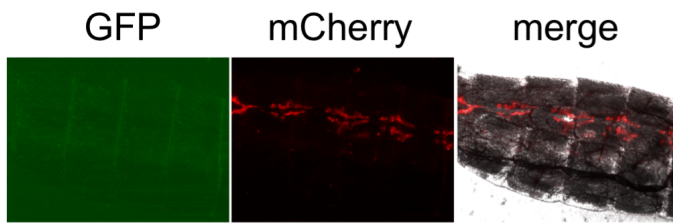


FigS5

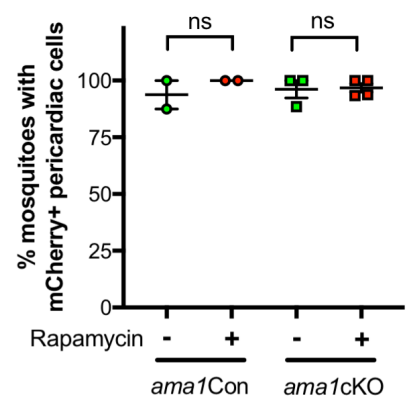


FigS6

A

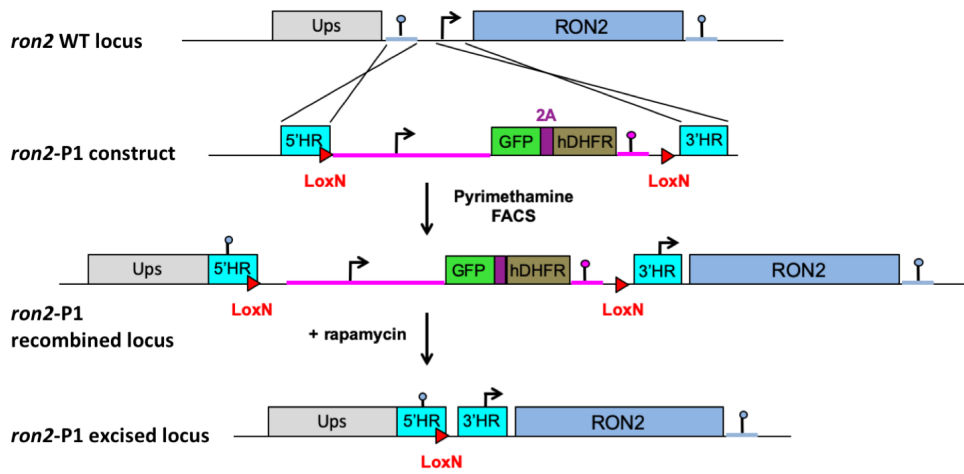


B

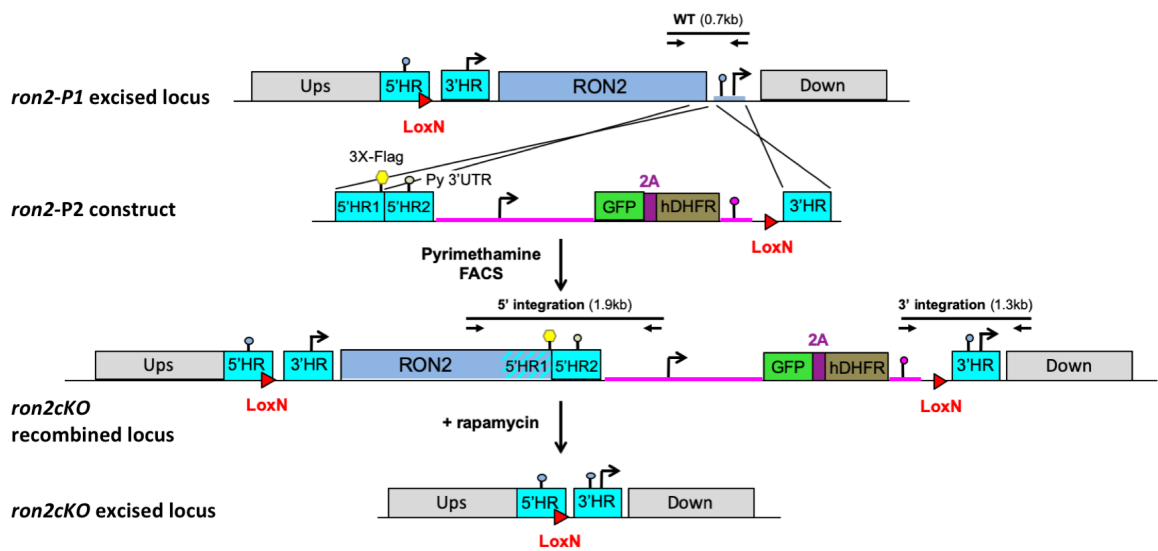


**FigS7**

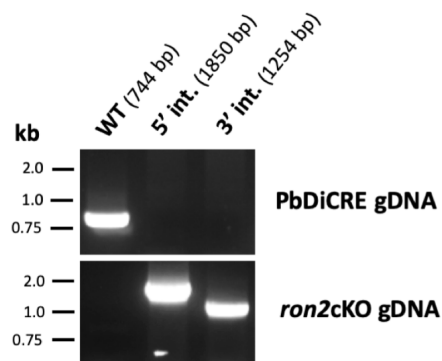
**A**



**B**

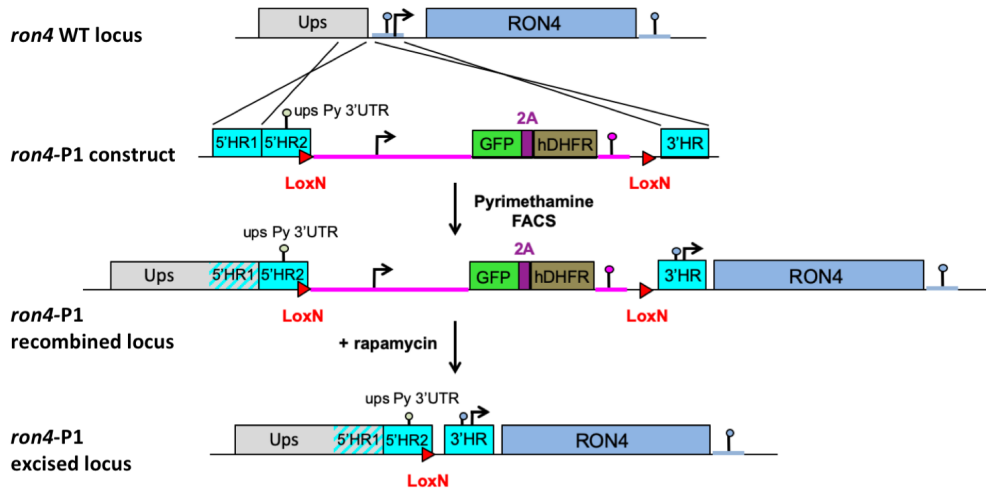


**C**

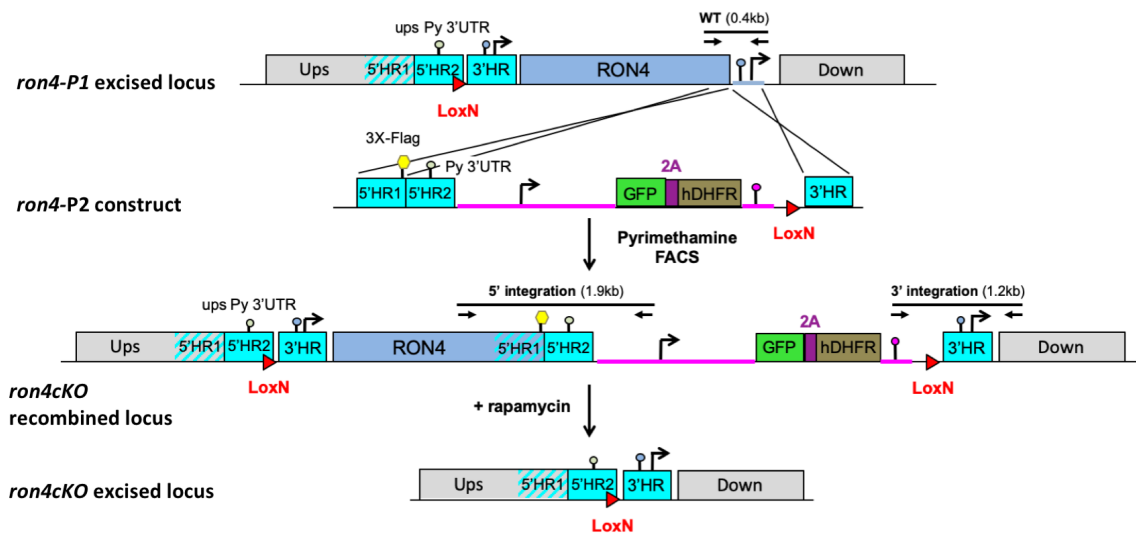


**FigS8**

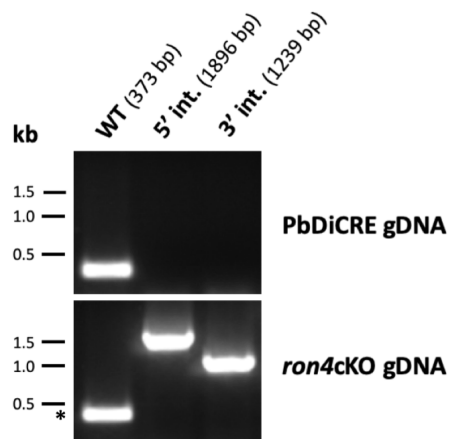
**A**



**B**

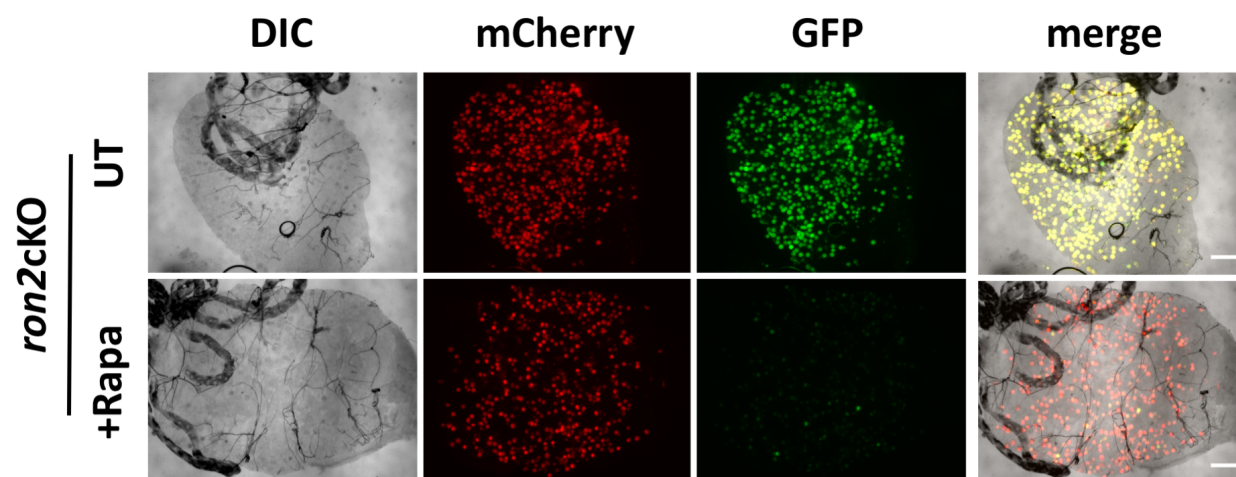


**C**

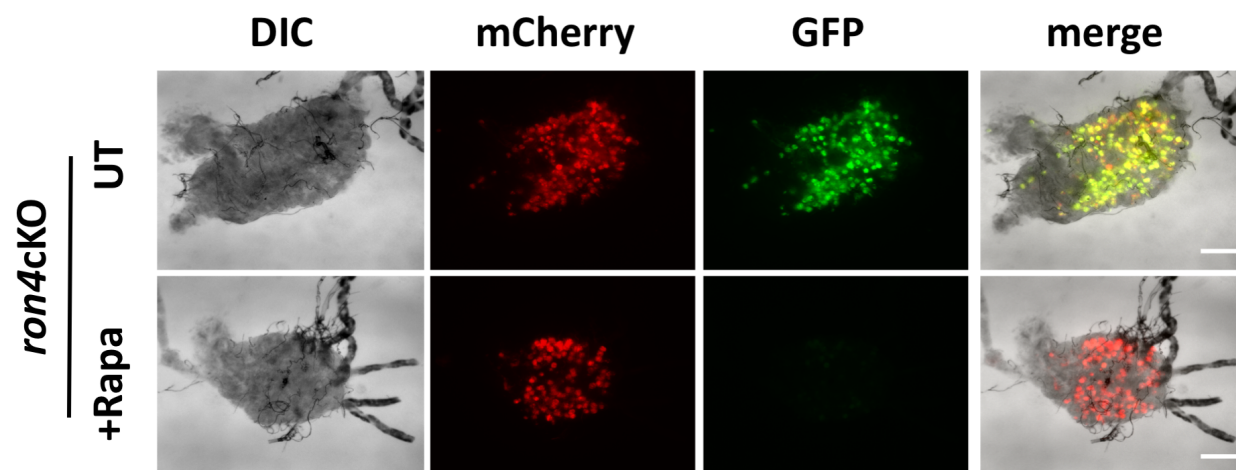


FigS9

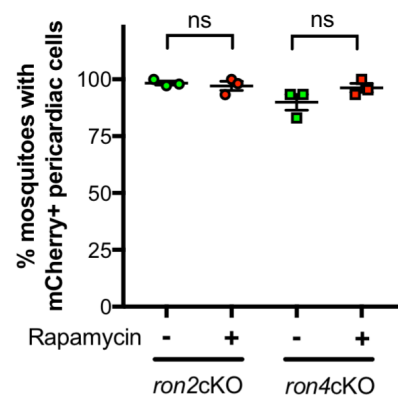
A



B

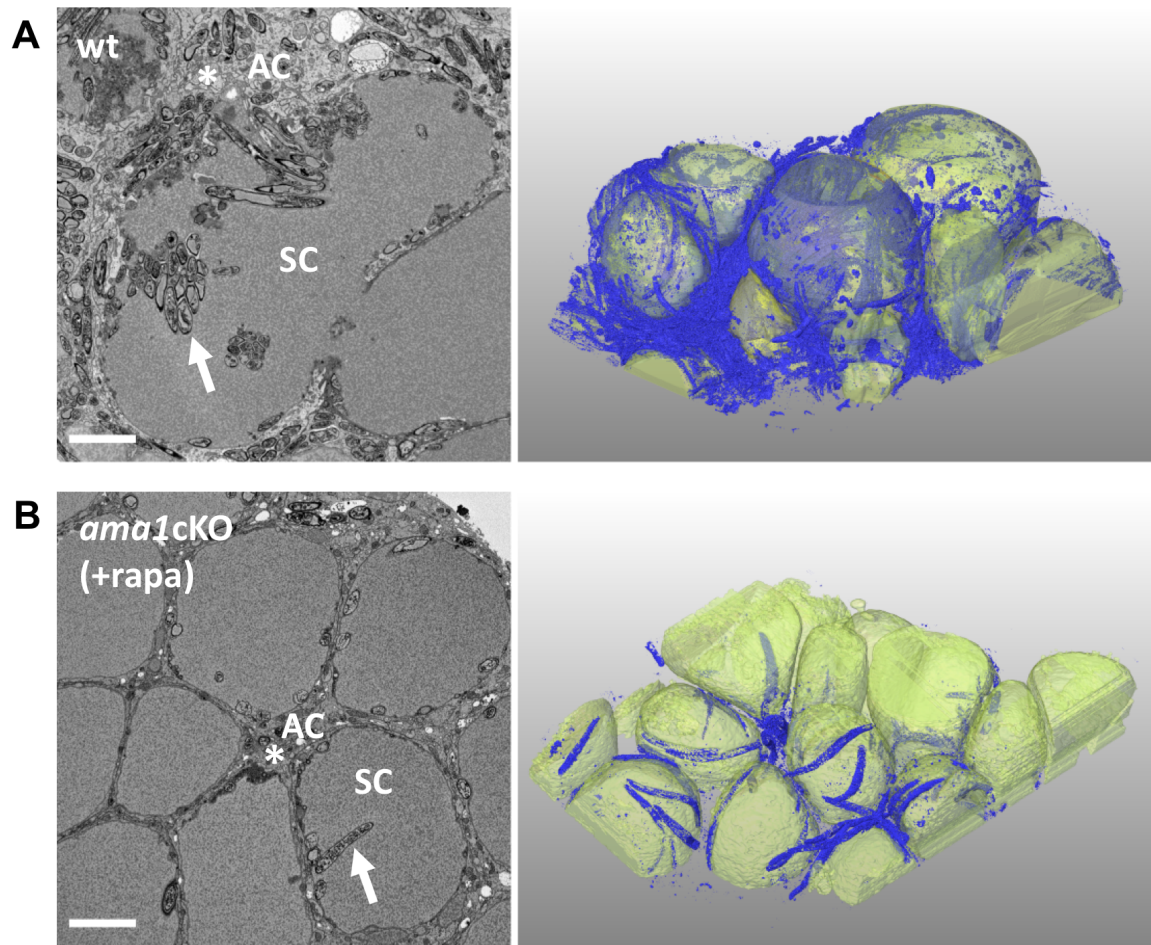


FigS10

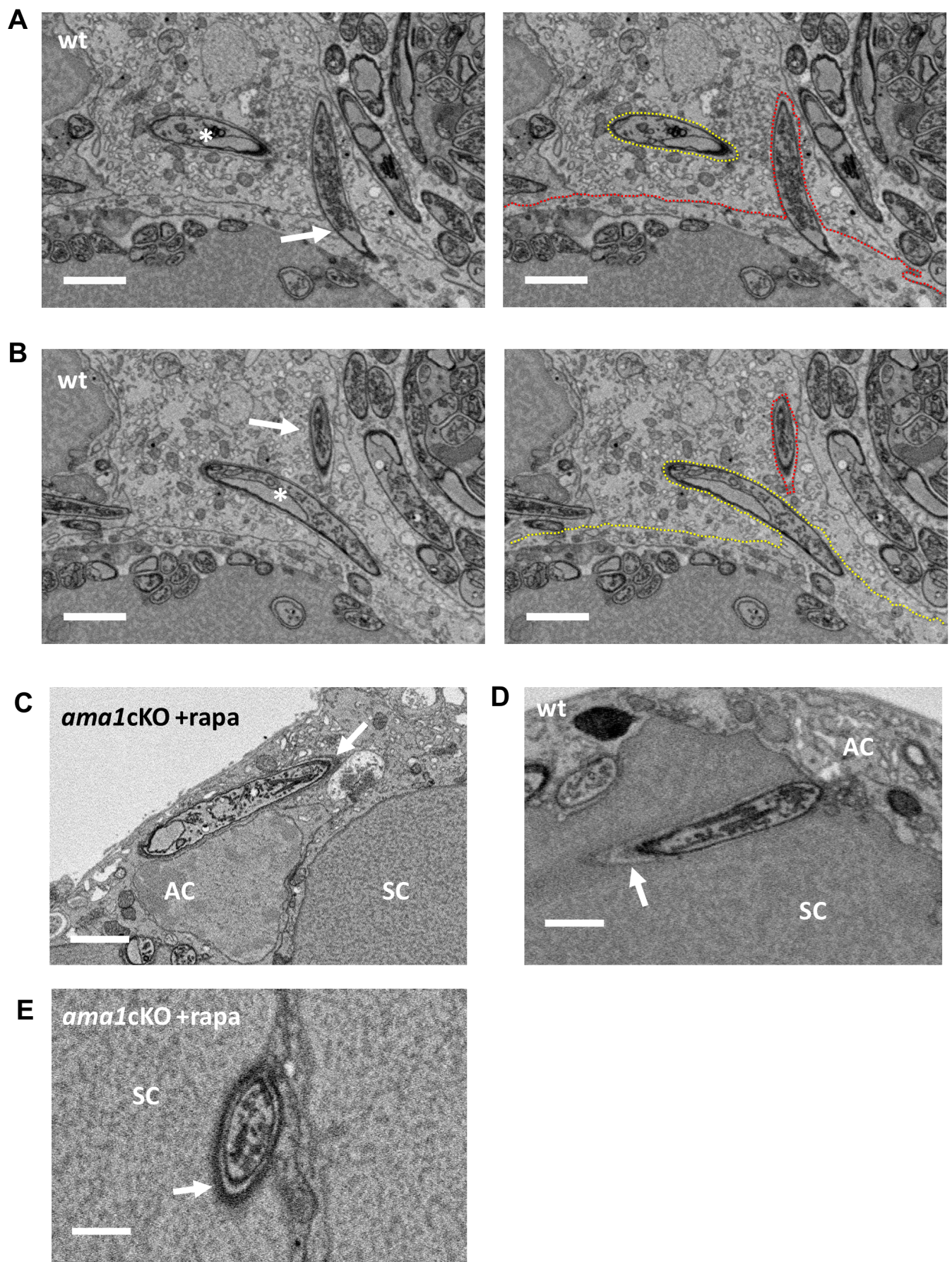




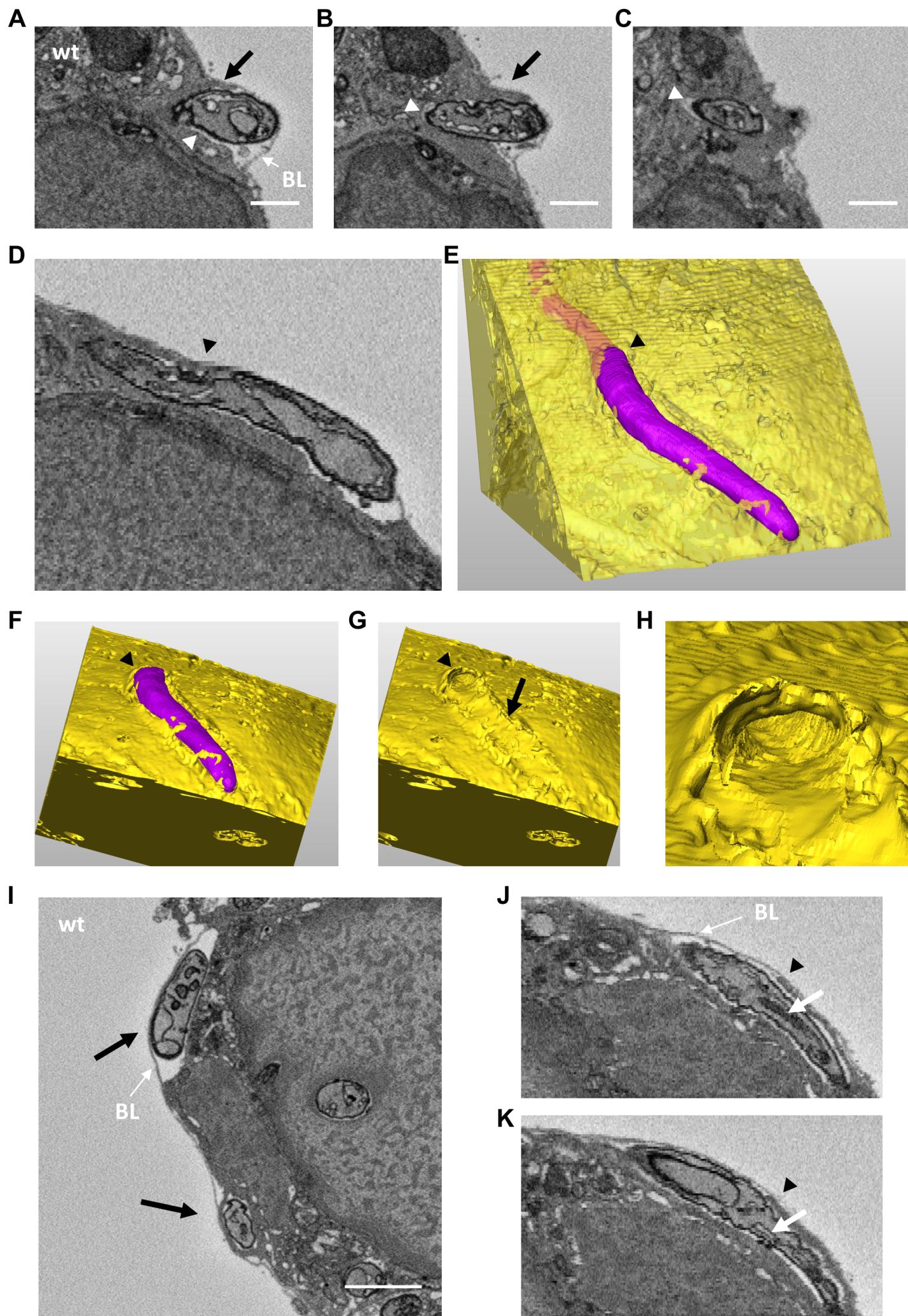
**FigS11**



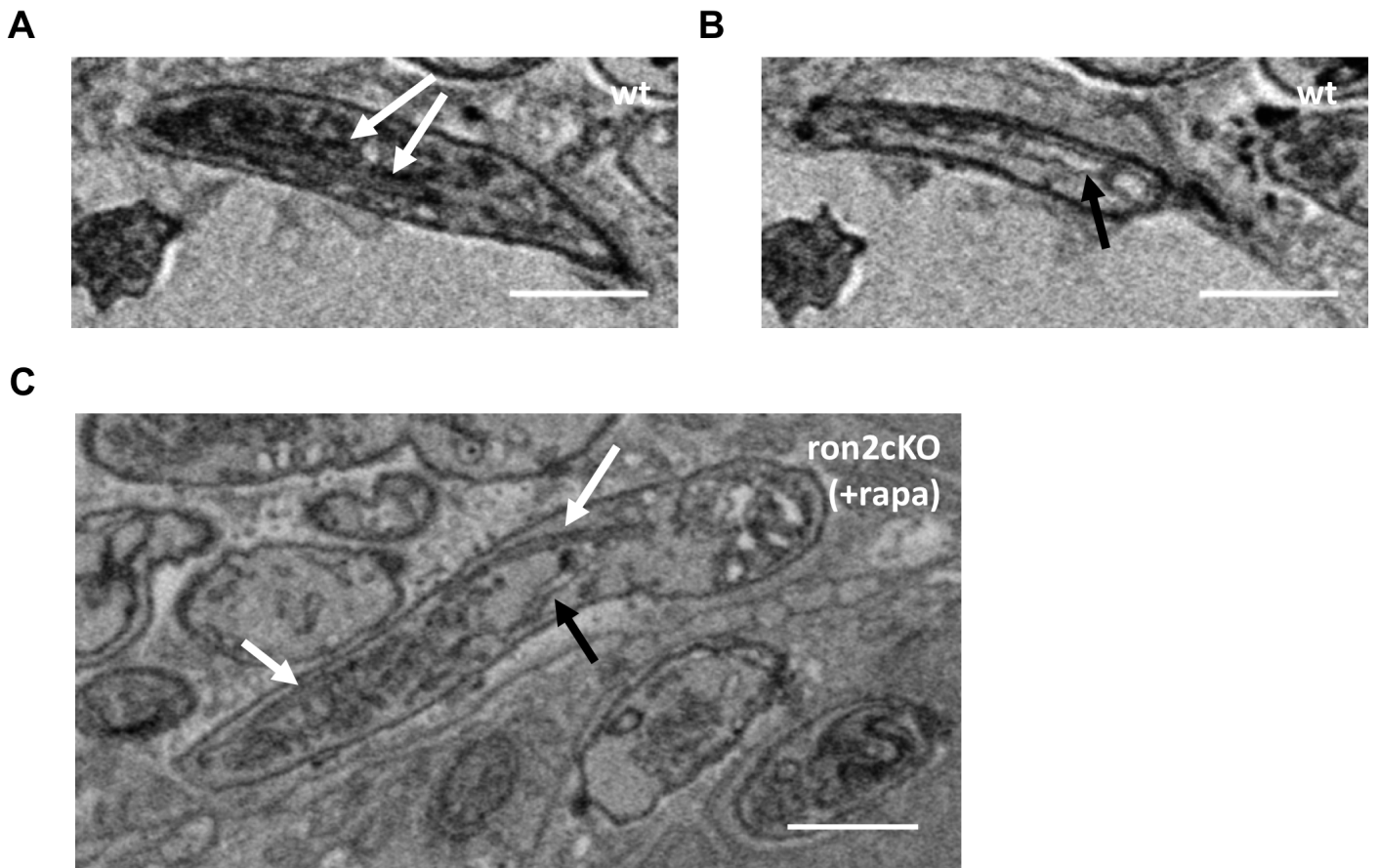
**FigS12**



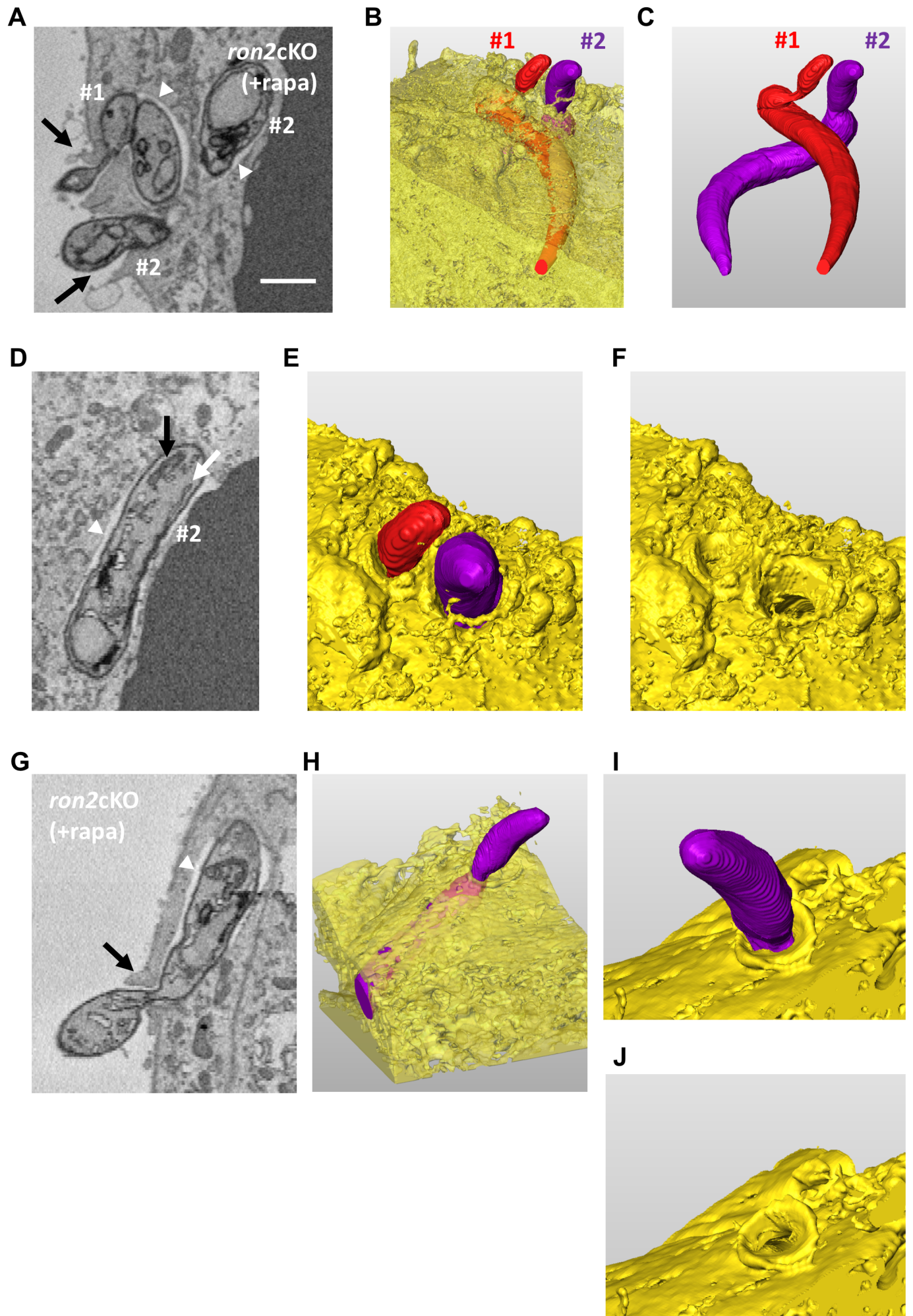
**FigS13**



**FigS14**

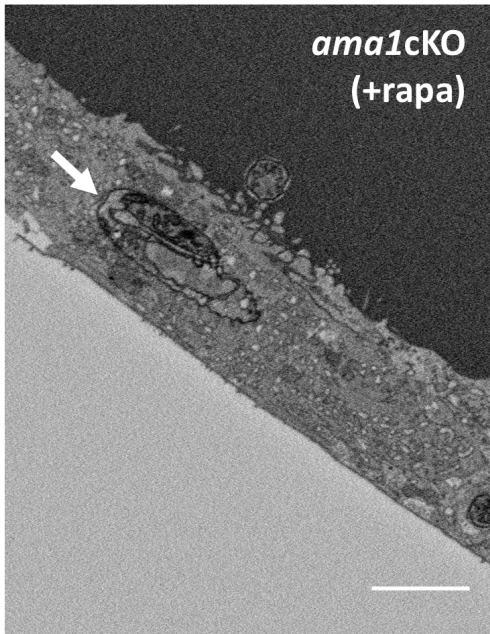


**FigS15**

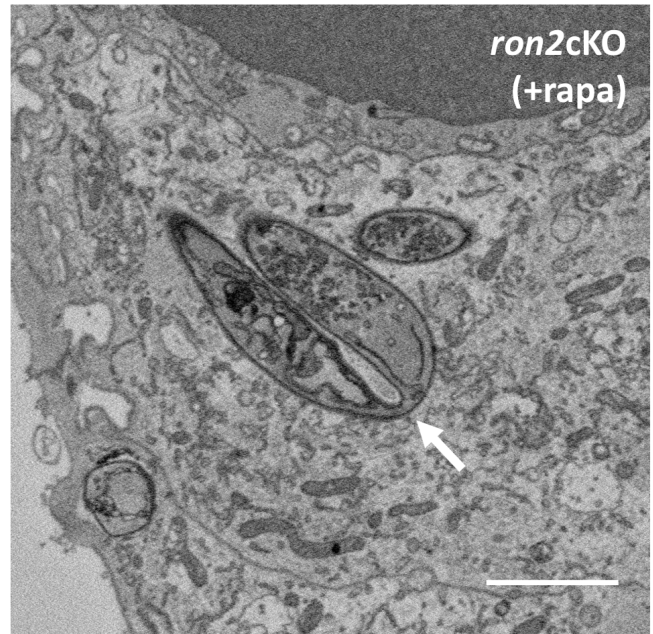


**FigS16**

**A**

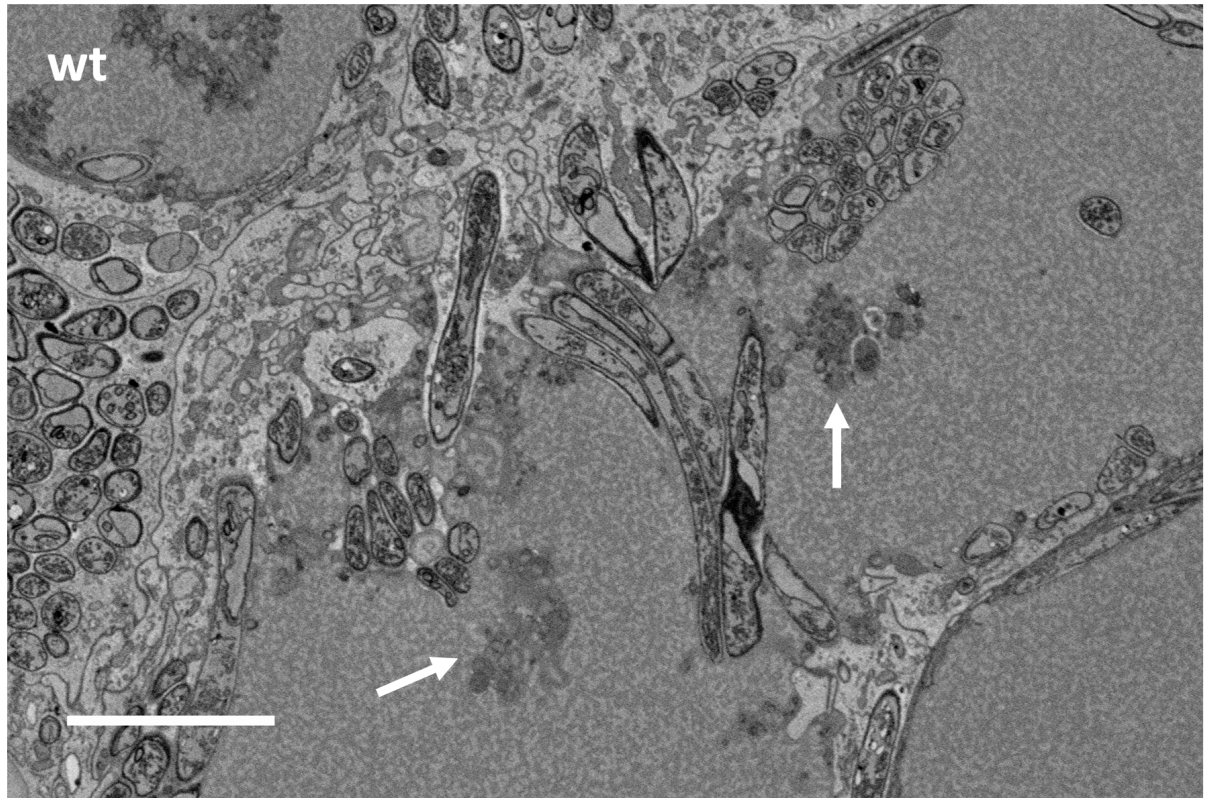


**B**

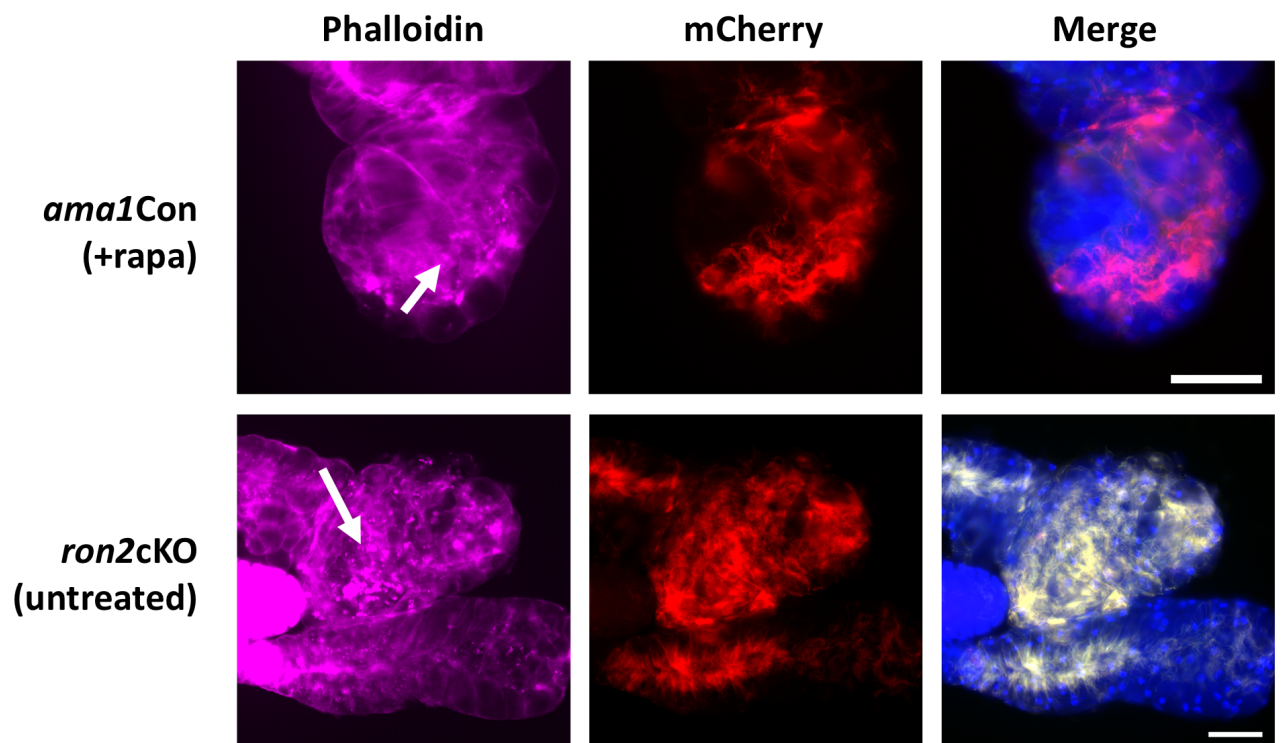


**FigS17**

**A**



**B**



FigS18

